MATERIALS CHEMISTRY
FRONTIERS

REVIEW

View Article Online
View Journal | View Issue



Cite this: *Mater. Chem. Front.*, 2023, **7**, 1704

# Phthalocyanine in perovskite solar cells: a review

Ehsan Rezaee,[ab] Danish Khan,[a] Siyuan Cai,[a] Lei Dong,[a] Hui Xiao,[a] S. Ravi P. Silva,[b] Xiaoyuan Liu*[a] and Zong-Xiang Xu*[a]

Presently, due to the rapid development of perovskite solar cells (PSCs), their commercialization is not only attractive but perhaps the only choice to replace both thin film photovoltaics (PV) and conventional silicon PV. However, although the power conversion efficiency (PCE) of PSCs is has reached above 25%, which is suitable for their commercialization, their poor long-term stability with scalability remains a challenge due to the sensitivity of perovskites under ambient conditions. Therefore, the top and bottom layers sandwiching the perovskite layer are critical. In this case, the charge transport layers (CTLs) not only enable charge extraction but also play the role of encrusting, passivating, and supporting the perovskite layer. Therefore, the perovskite interface has a dominant influence on the performances of PSCs. In this case, phthalocyanines (Pcs) have a large π-conjugated framework, outstanding thermal stability, excellent physical/chemical stability, low cost, and can be endowed with a tunable energy band, good carrier mobility, solubility in common solvents, and facile synthesis through their appropriate design, making them a robust charge selective layer, passivation layer or both in PSCs. In this review, we summarize the studies on the application of Pc compounds in PSCs, including dopant-free macrocycle molecules, from the perspectives of molecular engineering, doped hole transporting material (HTM), and employment of Pcs as additives in the perovskite layer or HTMs. This review provides helpful insight for further enhancing the efficiency of PSC devices, while improving their long-term operational life by utilizing Pc materials.

Received 29th December 2022,
Accepted 20th February 2023

DOI: 10.1039/d2qm01369j

rsc.li/frontiers-materials



## 1. Introduction

Perovskite solar cells (PSCs) are being intensively researched given that their power conversion efficiency (PCE) has reached 25.7%, exhibiting potential for commercialization in the near future.[1] However, although this remarkable PCE is the highest

[a] *Department of Chemistry, Southern University of Science and Technology, Shenzhen, Guangdong 518055, China. E-mail: liuxy2022@sustech.edu.cn, xu.zx@sustech.edu.cn*
[b] *Advanced Technology Institute, Department of Electrical and Electronic Engineering, University of Surrey, Guildford, Surrey GU2 7XH, UK*

**Ehsan Rezaee**

*Ehsan Rezaee is currently a Post-Doctoral Researcher in the Advanced Technology Institute, University of Surrey. He received his PhD in Inorganic Chemistry from the University of Mazandaran, Iran in 2014. Then, he moved to the Southern University of Science and Technology, in China as a Post-Doctoral Fellow. His research is mainly focused on material design for energy harvesting and conversion devices, such as perovskite solar cells and large-area perovskite solar modules.*

**Danish Khan**

*Danish Khan received his BS Degree in Electrical Engineering from COMSATS University Islamabad and his PhD in Renewable Energy from the North China Electric Power University in 2019. Currently, he is working as a Postdoc under the guidance of Prof. Zong-Xiang Xu. His current research focuses on developing stable and efficient perovskite solar cells.*

 

in the history of thin film photovoltaics, the commercialization of PSCs can only be realized by achieving long-term stability and scaling up their fabrication methods. Specifically, the performance of PSCs in two aspects, *i.e.*, stability and PCE, degrades when PSCs are scaled up.[2] The stability issues generally originate from the main absorber, *i.e.*, the perovskite layer, when it is exposed to ambient conditions.[3] At the beginning of the development of PSCs, many efforts were devoted to lengthening the lifetime of PSCs by adjusting the perovskite compositions and crystal structures. Subsequently, the charge transport layers (CTLs) were endowed with defect passivation and charge transportation properties given that the CTLs have direct interfacial contact with the perovskite layer. Accordingly, the interfaces of perovskite have become crucial, and in this case extra passivation layers have been incorporated to alleviate the built-in defects in perovskite and protect it from the external environment.[4] In general, PSCs can be divided into three basic architectures including positive–intrinsic–negative (p–i–n), negative–intrinsic–positive (n–i–p) and mesoporous n–i–p. Regardless of the architectures, the perovskite/CTL interface is an opportunity to counter the built-in defects in the bulk perovskite, at the surface, or in the grain boundaries. In addition, the interfacial contact between the adjacent layers directly influences the carrier extraction and recombination.[5] Therefore, numerous techniques such as compositional,[6] interfacial,[7] and passivation engineering[8] have been applied mainly through the interactions between the perovskite/CTLs. Nevertheless, another big concern is replacing the conventional hole transport materials (HTMs) ((2,2′,7,7′-tetrakis(*N*,*N*′-di-*p*-methoxyphenyl-amine)-9,9′-spirobifluorene (spiro-OMeTAD), poly[bis(4-phenyl)(2,5,6-trimethylphenyl)-amine] (PTAA), and poly-(3,4-ethylenedioxythiophene)-poly(styrenesulfonate)(PEDOT:PSS)) with new materials to enhance the cost-effectiveness and stability of the device, where small molecules can play a vital role.[9] Small molecules enable facile design modifications to achieve the required properties, such as dopant-free HTMs, interlayers, organic–inorganic hybrid HTMs or electron transport materials (ETMs), or as additives to improve the formation of perovskite crystals.[9,10] Conclusively, small molecules are beneficial to enhance the properties of the bottom, top, and perovskite layers. However, before the application of small molecules in PSCs, several factors need to be considered, such as their reproducibility, cost-effectiveness, solubility, stability, hydrophobicity, energy levels, and light absorption.[11] Generally, most of these properties are acquired through the selection of an appropriate molecular core, and then further design modifications are applied with regard to the specific device.[9] Besides these properties, the formation of a thin film with the desired structural and morphological characteristics is one of the main priorities, where conjugated π systems play a significant role.[12]

Phthalocyanines (Pcs), which are aromatic heterocyclic compounds derived from porphyrins, are among the most comprehensive π-conjugated system-based molecules.[13] They possess four isoindole units bridged by nitrogen atoms, forming a two-dimensional extended π-conjugated system with 18 delocalized electrons, which offers high thermal, chemical, and photostability for Pc materials.[14] This extended π-conjugated system also assists in the absorption of Pcs in

**S. Ravi P. Silva**

*S. Ravi P. Silva CBE FREng is a Distinguished Professor and the Director of the Advanced Technology Institute at Surrey University. He joined Surrey after completing his Undergraduate and Postgraduate degrees at Cambridge University. His research interests include nanotechnology and renewables. He is a Fellow, Royal Academy of Engineering, UK and Fellow, National Academy of Sciences Sri Lanka. He was made a Commander of the Order of the British Empire in the 2021 Queen's New Year Honours' list.*

**Xiaoyuan Liu**

*Xiaoyuan Liu received his PhD in Applied Chemistry from Nanjing Tech University in 2018. He completed his Postdoctoral research from 2018 to 2021 at the Pohang University of Science and Technology, Korea. After that, he joined the Southern University of Science and Technology as a Research Assistant Professor. His research interests focus on the design and synthesis of organic semiconductors as well as their application in perovskite solar cells.*

**Zong-Xiang Xu**

*Zong-Xiang Xu is an Associate Professor in the Chemistry Department of Southern University of Science and Technology. In 2008, Dr Xu received his PhD in Chemistry from the University of Hong Kong, and then joined the City University of Hong Kong, where he completed postdoctoral research between 2010 and 2012. Currently, his research is focused on the molecular design of materials and their applications in new energy harvesting, such as perovskite solar cells.*

the red/near-infrared (NIR) region of the solar spectrum, which exhibit two characteristic bands, *i.e.*, a Soret or B-band with a generally weaker absorption and intense Q-band with a molar extinction coefficient as high as 300 000 $M^{-1}$ $cm^{-1}$.[15,16] Subsequently, the ability to design and synthesize Pcs with different properties make this interesting class of macrocyclic organic compounds suitable for a variety of applications, including dyes and pigments, photocatalysts, imaging and therapy, chemical sensors, single-molecule magnets, and as active materials in electronic devices, such as organic photovoltaics (OPVs), thin-film transistors (OTFTs), light-emitting diodes (OLEDs), dye-sensitized solar cells (DSSCs) and PSCs.[17–21]

In addition to introducing various functional groups in Pcs as substituents, strategies based on the π–π interactions of Pc molecules and their orientations, electron–donor–acceptor (D–A) systems including Pcs and other electron active subunits, and covalent organic frameworks (COFs) were also developed in last two decades for the design and synthesis of novel Pc-based materials in the form of thin films, nanoparticles and other ordered condensed matters, which can be employed for the fabrication of devices with practical and potential applications.[22–28] The first report on the synthesis of a Pc was published in 1907 by Braun and Tchemiac.[29] They obtained a small amount of blue material as a by-product during the preparation of 2-cyanobenzamide, which was $H_2$Pc. However, at that time, they did not know the structure of the blue material, and therefore no name was given to it. Subsequently, a copper(II) Pc compound was synthesized in 1927 during the preparation of phthalonitrile.[30] Similarly, the structure of this dark blue material was not characterized. The structure of Pc compounds was first published in 1934, and further characterized by Robertson using X-ray diffraction analysis.[31–38] In the decade after the characterization of the first Pc compounds, a variety of strategies has been developed for the design and synthesis of many types of Pc compounds, dividing this class of interesting organic materials into several categories, including metal-free or metal-coordinated Pcs, unsubstituted and symmetrical or unsymmetrical substituted Pc compounds, binuclear, trinuclear, tetranuclear, pentanuclear and octanuclear Pcs, fused-Pcs and ball-type Pcs.[39–44]

Pcs, specifically in PSCs, are used as HTMs, interlayers or additives in the absorber films or HTMs. Pc-based HTMs with both structures (n–i–p or p–i–n) play a crucial role in enhancing the performance of PSCs. In n–i–p devices, they act as a protective layer on the perovskite, while in p–i–n, they act as a support for the deposition of the perovskite. The general trend is the use of PEDOT:PSS, PTAA or spiro-OMeTAD as HTMs in efficient PSCs. However, these conventional HTMs have serious drawbacks such as high cost, low reproducibility, hygroscopicity and dopant requirement.[45] These problems can be overcome through the use of Pcs derivatives owing to their high thermal stability, hydrophobicity and high hole mobility and conductivity. In addition, Pcs can be decorated with Lewis acid–base passivation capability and deposited on the perovskite as an interlayer or HTM. Lastly, as additives in the perovskite layer, Pcs enhance the film crystallinity and coverage and reduce the chance of defect generation in perovskites. At each position in the PSC device structure, the required properties of Pc compounds can be tuned by judiciously tailoring their structures. Pcs often strongly chelate to metals or metalloids of all groups of elements through two covalent and two coordination bonds, forming stable metal Pcs (MPcs).[46,47] Additionally, regarding the designed target for a Pc compound, different groups with various electronic and spatial structures can be introduced in either the Pc ring as substituents or the central ion as axial ligands, endowing it with new chemical and physical features. The substituted groups may also occupy the peripheral or non-peripheral positions on the Pc ring, resulting in different properties in the final compound (Fig. 1a and b).[48] For example, while applied as a dopant-free HTM, an improvement in the hole mobility can be achieved by enhancing the charge flow in the molecule in the form of electron–donor–acceptor (D–A) systems, intermolecular interactions *via* π-conjugation extensions or enhancement in the molecule planarity.[49–51] Another approach is perovskite defection passivation in the interlayer through the incorporation of Lewis bases at the appropriate position in the structure.[52] Furthermore, the approach of carrying two faces under one hood, *i.e.*, defect passivation and dopant-free HTM in a single layer, can be applied.[53]

Initially, when unsubstituted Pcs were demonstrated as HTMs or interlayers, they faced the issues of low solubility, low film coverage, and low hole extraction. These issues result in a low open circuit voltage ($V_{OC}$) and fill factor (FF), hindering the PCE. Accordingly, to overcome the problems of insolubility and low film coverage of Pcs, numerous fabrication techniques have been developed to coat thin film layers of Pcs. Consequently, the PCEs improved to a certain level. Furthermore, the decoration of tetra-substituted or octa-substituted Pcs with alkyl chains, diphenylamine (DPA), triphenylamine (TPA), thiophene, *etc.* resulted in many new properties in PSCs such as D–A properties, energy level optimization, defect passivation, dopant-free HTMs, solubility in different solvents, enhanced film morphology, *etc.* (Fig. 1a and b). Pcs are mostly incorporated as HTMs (below the perovskite layer in p–i–n devices and above the perovskite layer in n–i–p devices) and interlayers (above the perovskite layer) (Fig. 1c). All these positions are critical due to their direct contact with the sensitive perovskite. Hence, Pc compounds have been designed using different strategies such as enhancement of π-conjugation, inter or intra-charge flow by changing their center or arms, decoration with Lewis bases at the appropriate positions in their structure, or enhancement of planarity by changing the linkage positions or twisting angles of their arms. These designs govern the properties of Pcs such as solubility in organic solvents, film morphologies (perovskite and Pc-based layer), hydrophobicity, charge extraction, defect passivation, perovskite crystallization and hole mobility (Fig. 1d), which are essential for PSCs and can be optimized by substituting the necessary blocks around the Pc ring.

Due to their unique characteristics, Pc compounds have recently attract great attention in perovskite-related studies,

 

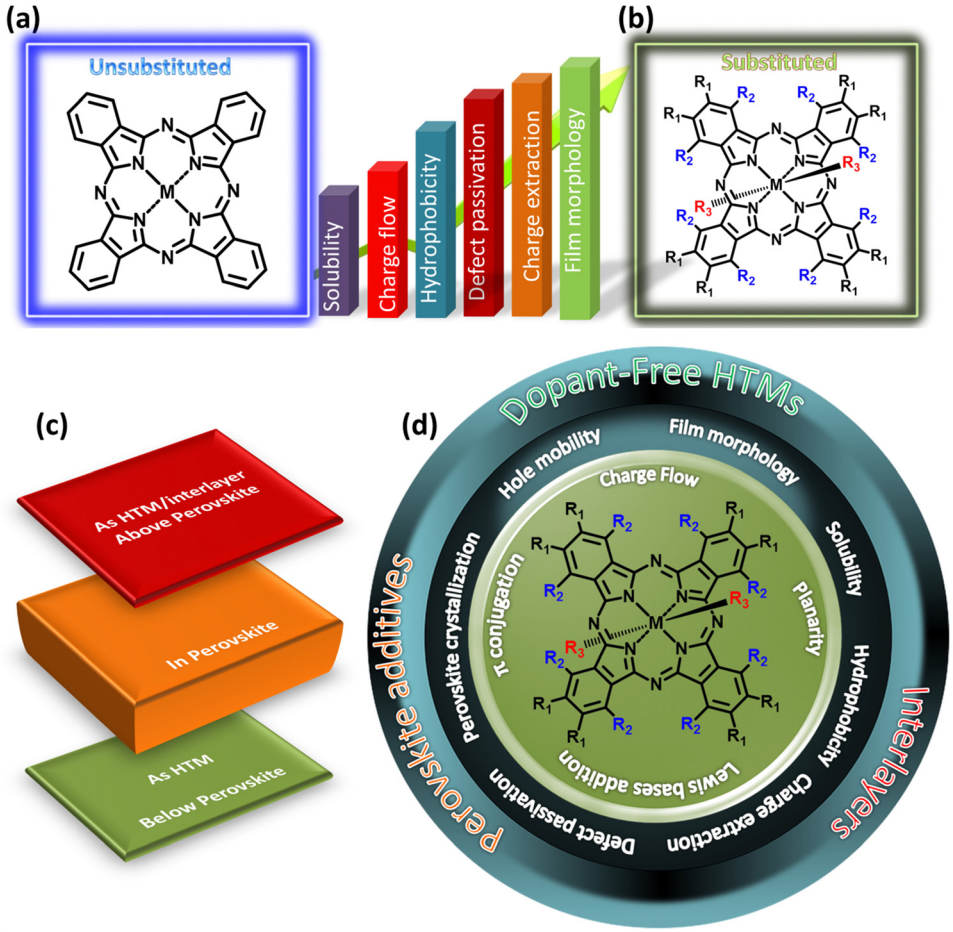


Fig. 1 (a) Unsubstituted Pc, (b) substituted Pc, (c) Pc applications in different layers of PSCs and (d) design strategies linking the important parameters of PSCs.

but there is a lack of reviews summarizing all the recent developments in the literature and highlighting the unique role Pc materials can play in the future commercialization of PSC devices. Therefore, this review aims to present the basis of the functionality of Pcs as certain layers in PSCs. In Section 2, we discuss the applications of Pc compounds in five categories, including molecular-engineered dopant-free HTMs in accordance with the quantity of substituent, doped Pc, interfacial modification layer, and Pc acting as an additive in the perovskite film and HTMs. Finally, we present some remarks and conclusions. The aim of this study is to provide readers with comprehensive information about the applications of Pc materials and the most notable achievements to date.

## 2. Application of phthalocyanines in PSCs

### 2.1. Dopant-free phthalocyanine-based HTMs for PSCs

**2.1.1. Unsubstituted Pc materials.** In multilayer film devices, pristine metal phthalocyanines easily aggregate through π–π stacking interactions, resulting in high hole mobility and conductivity, which make them suitable to obtain high-performance perovskite solar cells. However, they are barely soluble in common organic solvents such as chlorobenzene and dichlorobenzene, limiting their use as a single HTM in PSCs unless adopting relatively high-cost thermal vacuum deposition methods. To date, although Pc materials have been established to exhibit a satisfactory performance as semiconducting dyes in OPVs, the first report on the use of a Pc material as an HTM in a PSC device was only published in 2014.[54] In the study by Lianos *et al.*, they employed an unsubstituted copper(II) phthalocyanine (CuPc) as a dopant-free HTM in a mesoscopic PSC, and the highest PCE of 5.0% was achieved. In the following year, Fang and coworkers significantly enhanced the efficiency of CuPc-based devices and achieved the PCE of 15.43% for the PSCs with a thin layer of C60 as an electron transporting material (ETM).[55] They observed that the CuPc film could absorb light in the wavelength range of 550–750 nm, influencing the light absorption intensity by the perovskite layer, and consequently decreasing the final efficiency of the PSC device. In addition, a thick CuPc film can induce a larger series resistance and reduce the FF value of the PSC. Alternatively, a thin layer of CuPc cannot offer full coverage over the perovskite layer, resulting in shunt paths and poor hole extraction and electron blocking ability. Thus, by

optimizing the thickness of the CuPc thin layer, devices with effective hole extraction and electron blocking and with subsequent low interface recombination have been fabricated, exhibiting an improved FF value. In 2016, Sun and coworkers employed a nanorod-like unsubstituted CuPc as an HTM, together with a printable carbon cathode in a mesoscopic PSC device, which achieved an efficiency of 16.1%.[56] The developed HTM had a matched energy level with the perovskite layer and exhibited remarkably stronger hole extraction ability compared with the spiro-OMeTAD HTM. The PSC device exhibited improved $V_{OC}$ and short-circuited current density ($J_{SC}$) values. Torabi *et al.* fabricated a needle-like structure as a CuPc thin film by heating the substrate to 100 °C ± 5 °C during the thermal deposition process. Using the needle-like CuPc material crystallized in the α-phase monoclinic structure in the thin film state as a dopant-free HTM in a mesoscopic device with an Au electrode, a PCE of 14.89% was achieved.[57] It was suggested that the needle-like CuPc could offer a large interfacial contact area with the perovskite film, which resulted in a higher hole extraction ability for the HTM layer. Thus, due to these high efficiencies and great potential to realize device stability, unsubstituted CuPc attracted more attention in 2018. Liao *et al.* fabricated PSC devices with an inverted planar structure on both rigid and flexible substrates using a room temperature-evaporated CuPc thin film as an HTM and achieved PCEs of up to 15.4% and 12.8% for rigid and flexible devices, respectively.[58] With the established high performance of the CuPc HTM, the same group continued their research on optimizing the device performance by focusing on other active layers in the device and achieved an improved PCE of 16.72% for an inverted planar PSC, employing a cesium-containing triple cation perovskite as the light absorbing material, CuPc as the HTM and C60 with the optimized thickness of 18 nm as the ETM.[59] However, the performance of PSCs with the same architecture and deposited on flexible polyethylene terephthalate (PET) substrates only exhibited a PCE of 12.96%. Liao's research group achieved an efficiency of 15.39% for PSCs with a conventional structure, using CuPc as a dopant-free HTM, $TiO_2$/$SnO_2$ bilayer as the ETM, and a carbon counter electrode.[60] Also, they successfully extended the proposed device structure to a tandem module. Their research confirmed the versatility of applying CuPc materials in PSCs with different architectures and on different substrates. Employing a doping strategy for the fabrication of the ETM layer, they continued their work on CuPc-based PSCs with carbon counter electrodes. Also, planar perovskite devices with Mg-doped and Ni-doped rutile $TiO_2$ as the ETM were fabricated.[61,62] The devices based on Mg-doped $TiO_2$ ETM reached the PCE of 15.73%. Ni-doping could also enhance the charge mobility of the $TiO_2$ thin film by shifting the Fermi level of the ETM upward, resulting in an optimized PCE of 17.46%. Importantly, it was demonstrated that without the application of the CuPc-based HTM, the best-performing Ni-doped $TiO_2$-based device obtained a PCE of 10.79%. The decreased performance of the devices without the CuPc hole transport layer (HTL) can be mainly attributed to the fact that the interfacial energy barrier at the perovskite/top electrode interface impedes the charge-collecting efficiency of carbon and causes undesirable charge accumulation at the interface. Furthermore, the use of highly stable CuPc and commercial carbon led to excellent stability in the fabricated PSC devices, with no obvious decline in PCE after being stored in ambient air for 1200 h. This work presents an important step toward the commercialization of carbon-based PSCs with high efficiency and long-term stability. Wu *et al.* designed a bilayer HTM for inverted PSCs, consisting of an inorganic $VO_x$ matrix and CuPc buffer layer.[63] The fabricated devices showed PCEs of up to 16.85% with negligible hysteresis and high stability. The improved performance of PSCs using the developed bilayer HTM compared with the reference cell based on PEDOT originated from the appropriate energy level matching at the HTM/perovskite interface and excellent conductivity of the HTM. In 2019, Liao's group pushed the efficiency of perovskite devices based on dopant-free unsubstituted CuPc HTM to higher values.[64] The PSCs using the optimized Zn-doped $SnO_2$ ETM, vacuum-deposited CuPc HTM, and a carbon counter electrode achieved the highest PCE of 17.78%. The cross-sectional scanning electron microscopy (SEM) image of the fabricated device is presented in Fig. 2a, showing the well-defined structure of the PSC with the FTO/Zn:$SnO_2$/perovskite/CuPc/carbon configuration. Interestingly, most of the perovskite grains are formed perpendicular to the substrate, which favors efficient charge extraction and transfer. The *J–V* characteristics of the best-performing devices employing either an $SnO_2$ or Zn-doped $SnO_2$ film as the ETM layer are depicted in Fig. 2b. The PSC with the doped $SnO_2$ ETM showed $V_{OC}$, $J_{SC}$, and FF values of 1.098 V, 23.4 mA $cm^{-2}$, and 69.2%, respectively, offering an efficiency as high as 17.78%. Employing a CuPc HTM together with a carbon electrode could significantly enhance the device stability. The fabricated PSCs could maintain 100% of their initial performance after storage in air for 1200 h (Fig. 2c). The excellent stability can be ascribed to the hydrophobic nature of the CuPc and carbon layers, which is expected to protect the perovskite from moisture. In 2021, Tavakoli *et al.* fabricated inverted PSCs through all-vacuum processing, using CuPc as the HTL, reaching an efficiency as high as 20.3%, which is significantly higher than the PCE (16.8%) of the devices based on solution-processed CuPc.[65] This is attributed to the better charge extraction and transfer ability of the evaporated CuPc. The prepared PSCs also exhibited superior operational stability with only 9% loss in performance over 100 h under illumination. The PSCs prepared using the same method on PET achieved a PCE of 18.68%. In a recent study, Seok and coworkers discussed the necessity of using an interlayer between the perovskite film and CuPc, which helped in improving the $V_{OC}$ by blocking electron transfer at perovskite/CuPc.[66] Although the n–i–p devices using spiro-OMeTAD as the HTL could achieve the PCE of 21.41%, the CuPc-based PSCs with no interlayer showed an efficiency of 16.55%. Therefore, a wide band gap material, poly(methyl methacrylate) (PMMA), was inserted between the perovskite and CuPc to simultaneously improve the electron blocking ability of CuPc and protect the perovskite against oxygen and moisture. PMMA

 

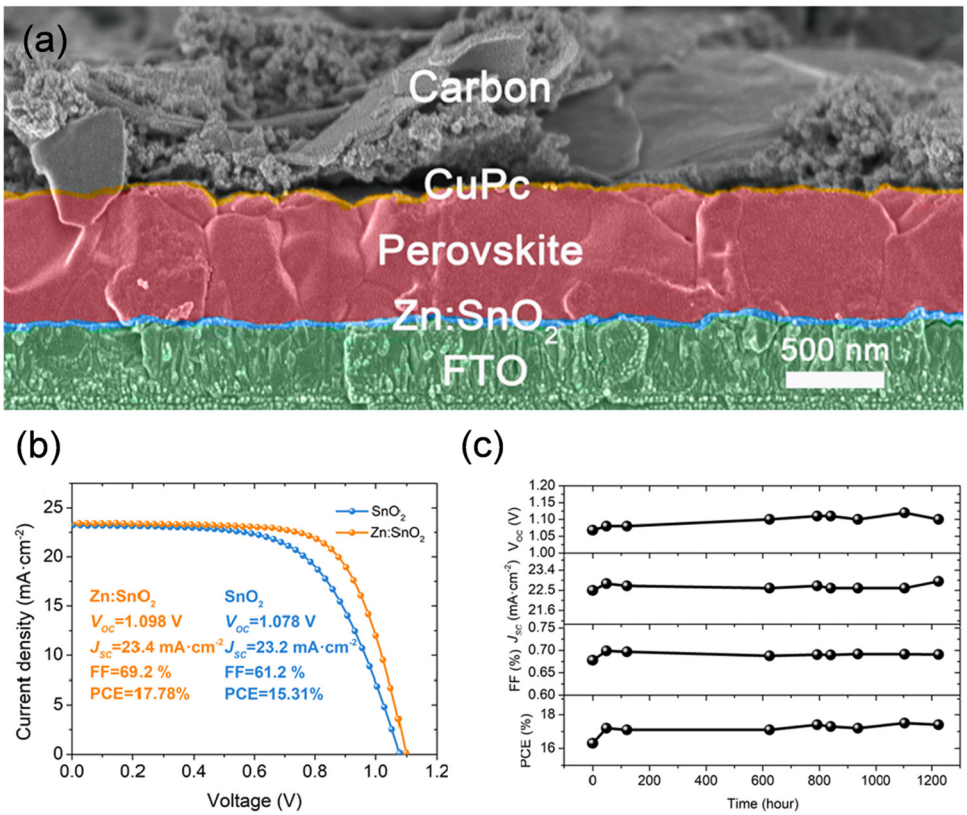


Fig. 2 (a) High-resolution cross-sectional SEM image of the carbon-based planar-structured PSC, (b) $J$–$V$ curves of the best-performing PSC with $SnO_2$ or Zn-doped $SnO_2$ as the ETM, (c) and evolution of the $J$–$V$ parameters of the Zn-doped $SnO_2$-based devices stored in the ambient air with a relative humidity of ~20%. Reproduced with permission.[64] Copyright 2019, Elsevier.

could also improve the film quality of CuPc by reducing the observed cracks and blocking the contacts between the top electrode and perovskite film. Due to the enhanced $V_{OC}$ and FF, the PMMA-added devices showed a significant jump in performance, reaching the PCE, $V_{OC}$, $J_{SC}$, and FF values of 21.25%, 1.08 V, 24.87 mA $cm^{-2}$, and 79.29%, respectively, when a 0.75 M PMMA solution in chlorobenzene was used in the device fabrication process. The photovoltaic properties of some selected perovskite devices using unsubstituted Pc compounds as the HTM layer are summarized in Table 1.[54–72]

Changing the metal center in Pc materials can alter their electronic and structural properties dramatically. Unsubstituted Pcs with metal centers, such as Zn, Pb, Ni, Sn, VO, and $TiO_2$, have been employed as the HTM in PSCs. In 2015, Di

Table 1 Photovoltaic properties of some selected perovskite devices employing unsubstituted Pcs in their structure

| Device architecture | HTM | Hole mobility of HTM ($cm^2$ $V^{-1}$ $s^{-1}$) | $V_{OC}$ (V) | $J_{SC}$ (mA $cm^{-2}$) | FF (%) | PCE (%) | Ref. |
|---|---|---|---|---|---|---|---|
| Mesoscopic | CuPc | — | 0.75 | 16.3 | 40 | 5.0 | 54 |
| Planar, n–i–p | CuPc | $\sim 10^{-2}$ | 1.04 | 19.13 | 77.74 | 15.42 | 55 |
| Mesoscopic | Nanorod-like CuPc | — | 1.05 | 20.8 | 74.0 | 16.1 | 56 |
| Mesoscopic | Needle-like CuPc | — | 1.04 | 20.14 | 71.0 | 14.89 | 57 |
| Inverted planar | CuPc | — | 1.03 | 19.4 | 77 | 15.4 | 58 |
| Inverted planar | CuPc | — | 1.075 | 20.63 | 75.4 | 16.72 | 62 |
| Planar n–i–p | CuPc | — | 0.98 | 23.28 | 67 | 15.39 | 60 |
| Planar n–i–p | CuPc | — | 1.025 | 22.26 | 68.9 | 15.73 | 59 |
| Planar n–i–p | CuPc | — | 1.073 | 22.41 | 72.6 | 17.46 | 61 |
| Inverted planar | CuPc/$VO_x$ | — | 1.015 | 22.15 | 74.8 | 16.85 | 63 |
| Planar n–i–p | CuPc | — | 1.098 | 23.4 | 69.2 | 17.78 | 64 |
| Inverted planar | CuPc | — | 1.108 | 23.34 | 78.5 | 20.30 | 65 |
| Planar n–i–p | PMMA/CuPc | — | 1.08 | 24.87 | 79.29 | 21.25 | 66 |
| Mesoscopic | ZnPc | $1.9 \times 10^{-3}$ | 0.83 | 22.8 | 43.4 | 8.13 | 67 |
| Inverted planar | ZnPc | — | 0.96 | 17.26 | 70 | 11.6 | 68 |
| Mesoscopic | TiOPc | — | 0.737 | 12.86 | 54 | 5.05 | 69 |
| Planar n–i–p | NiPc | — | 0.94 | 17.64 | 73 | 12.1 | 70 |
| Inverted planar | NiPc | — | 1.0 | 19.45 | 73.6 | 14.31 | 71 |
| Inverted planar | CuI/PbPc | — | 0.80 | 20.49 | 66 | 10.79 | 72 |

Carlo and coworkers employed ZnPc as dopant-free HTM in PSCs and reported an efficiency as high as 8.13% for a small area device with a mesoporous $TiO_2$ ETM.[67] They suggested that the orientation and stacking direction of the ZnPc molecules could significantly affect the electrical and optical properties. The vacuum-deposited α-phase ZnPc HTM with a thickness of 100 nm offered a hole mobility of around $1.9 \times 10^{-3}$ $cm^2$ $V^{-1}$ $s^{-1}$. The comparison of the incident photo-to-current efficiency (IPCE) spectra of the devices using ZnPc and spiro-OMeTAD as the HTM layers confirmed the contribution of ZnPc to the free charge generation process inside the PSC device. The ZnPc layer could also act as a shield layer for the perovskite against both light radiation and ambient moisture. A year later, Fostiropoulos *et al.* improved the PCE of the ZnPc-based PSC to 11.6% by using an ultrathin (5 nm) vacuum-deposited ZnPc HTM in an inverted perovskite device.[68] In their study, a two-step vacuum deposition process was used for the fabrication of the perovskite layer and the film quality was improved by optimizing the deposition rate. Li and coworkers used titanylphthalocyaine (TiOPc) as an HTM for PSCs with a mesoscopic configuration. Specifically, β-form and α-form TiOPc HTMs were fabricated *via* thermal vapor evaporation under vacuum and solvent annealing, respectively. The β-form TiOPc as the HTM achieved a higher PCE of 5.05% than the α-form, which can be attributed to the better thin film morphology and matching energy level of the HOMO.[69] Haider *et al.* employed unsubstituted NiPc as a dopant-free HTM in a planar n–i–p-structured PSC for the first time and achieved PCEs of 12.1% and 6.2% for small and large area devices, respectively.[70] NiPc showed excellent hole extraction ability from the perovskite active layer, with a relatively high hole mobility of $1.0 \times 10^{-1}$ $cm^2$ $V^{-1}$ $s^{-1}$. The use of thermal evaporation deposition allowed the small-size NiPc to permeate into the perovskite grain boundaries and improve the efficiency of hole extraction due to the enhanced interface contact. The thickness of the NiPc layer was also optimized, with a 120 nm film achieving the highest performance. The photoluminescence (PL) and impedance spectroscopy studies indicated that the NiPc layer could offer superior hole extraction and transfer ability compared with the CuPc thin film. In another study by the same group in 2019, pristine NiPc was employed as an HTM in an inverted PSC and a PCE of 14.3% was reported, indicating the potential of NiPc materials for the fabrication of different PSC architectures, which can compete with CuPc as the typical representative of MPc-based HTMs.[71] To achieve the best performance for the inverted perovskite devices, the NiPc HTM thickness was optimized to 30 nm, where the undesirable direct contact between the perovskite layer and the transparent electrode, the reduced incident light transmittance, and the increased series resistance were all avoided. Hou *et al.* used unsubstituted PbPc in a p–i–n-structured PSC fabricated under high humidity conditions.[72] In their work, PbPc on a thin CuI layer was used as the HTM in PSCs with inverted structures. The hydrophobicity of the PbPc was beneficial for the formation of a porous $PbI_2$ film and the fast preparation of a compact and homogeneous perovskite film with a large grain size. Consequently, reduced absorption in the visible area was achieved for the CuI–PbPc layer, which was critical in maintaining the light absorption level of the perovskite layer, especially in an inverted PSC device. The prepared devices showed a PCE of 10.79%, which is comparable with PEDOT:PSS-based PSCs, with good long-term stability.

MPc materials offer a large and fully conjugated aromatic framework and high thermal and chemical stability. They can be thermally evaporated over large areas and are suitable for the fabrication of both small and large area perovskite devices. Altering the metal center in MPc compounds can adjust their characteristics, such as electronic and optical properties, charge transfer ability, carrier diffusion length, and solid-state molecular alignment, which make them suitable choices for various tasks. Studies have established the compatibility of these materials for various device structures and their unique potential to act as either the underlying smooth thin film or the capping shield layer for the light absorbing perovskite film in PSCs. However, it is worth noting that in a conventional n–i–p PSC, Pc materials can also help PSC devices to absorb light in the wavelength range of 550 to 800 nm as a result of their wide Q band absorption. Therefore, the low energy photon penetrating perovskite layer can be absorbed by the Pc-based HTM layer and the photogenerated electrons in the Pc thin film can be injected into the perovskite layer to enhance the PCE of the device.

**2.1.2. Tetra-substituted Pc materials in PSCs.** The introduction of substituents in Pc macrocycles is another strategy employed to modify their characteristics, such as enhancing the solubility of Pc materials and their overall stability, improving the thin film morphology of Pcs and modulating their optoelectronic and electrochemical properties. In 2016, the Lianos team and our group introduced four methyl groups as peripheral substituents in CuPc and explored the performance of the substituted Pcs as HTMs in PSCs.[73] Although the addition of methyl groups to CuPc did not significantly enhance its solubility in common organic solvents, it had some impact on its molecular packing patterns, and consequently the charge mobility in the CuMePc (**1**) thin film. The authors compared the performance of the CuMePc-based PSCs with their unsubstituted counterparts, and a slight enhancement was observed in the overall performance of the substituted Pc-based device. The PSCs with CuMePc as the dopant-free HTM exhibited an efficiency of up to 5.2%, while the unsubstituted CuPc-based perovskite devices achieved a PCE of 5.0%. However, methyl substitution was only the first step, and this strategy was followed by more drastic substitution to develop soluble Pc-based HTMs for PSCs. Our research group developed PSCs with the n–i–p planar architecture, employing an $SnO_2$ thin film as the ETM and unsubstituted and tetra-methyl- and tetra-ethyl-substituted CuPc as the HTMs.[74] The results from the field-effect transistor (FET) and space-charge-limited-current (SCLC) methods confirmed the higher hole mobility of CuMePc and CuEtPc (**2**) than CuPc. This was attributed to the shorter stacking distances and stronger intermolecular face-to-face π–π interactions of the Pc rings in CuMePc and CuEtPc compared with CuPc. With the new device structure, PCEs of 9.1%, 11.7%,

 

and 11.5% were achieved for the devices using CuPc, CuMePc and CuEtPc as dopant-free HTMs, respectively. In 2018, conventional planar PSCs utilizing peripherally tetra-propyl-substituted CuPc (CuPrPc, **3**) as a dopant-free HTM were fabricated by our group, and the highest PCE of 17.8% was reported.[75] A high-quality CuPrPc thin film was fabricated *via* solution-processed methods and formed a face-on molecular orientation on the perovskite layer, which was ideal for higher out-of-plane conductivity and hole mobility. This was also projected in the high $J_{SC}$ values obtained for the devices. CuPrPc could also improve the stability of the PSC devices through its good film coverage and high hydrophobicity. The photovoltaic properties of some selected perovskite devices using tetra-substituted Pc compounds as the HTM layer are summarized in Table 2.[50,53,73–96] The molecular structures of the Pc materials used as dopant-free HTMs in PSCs are shown in Fig. 3. Continuing our study on employing tetra-propyl-substituted Pc compounds, we replaced the Cu metal ion with Zn and Pd and fabricated PSC devices using ZnPrPc (**4**) and PdPrPc (**5**) as dopant-free HTMs, respectively.[76] It was argued that the observed lower PCE of the MPc-based PSCs compared with perovskite devices using the state of art spiro-OMeTAD originated from the narrow bandgap (in the range of 1.6–2.0 eV) of the MPcs, which resulted in poor electron blocking and higher charge recombination. Employing a heavy atom with 4d and 5d valence orbitals, such as Pd, in MPcs can offer strong spin–orbit coupling and improve the intersystem crossing (ISC) rate of singlet to triplet excitons, which have a longer lifetime.

Table 2 Photovoltaic properties of some selected perovskite devices employing tetra- and octa-substituted Pcs as dopant-free HTMs

| Chemical structure no. | Device architecture | HTM | Hole mobility of HTM ($cm^2\ V^{-1}\ s^{-1}$) | $V_{OC}$ (V) | $J_{SC}$ (mA $cm^{-2}$) | FF (%) | PCE (%) | Ref. |
|---|---|---|---|---|---|---|---|---|
| **1** | Mesoscopic | CuMePc | — | 0.70 | 16.9 | 40 | 5.2 | 73 |
| **1** | Planar n–i–p | CuMePc | $1.95 \times 10^{-3}$ | 0.968 | 23.11 | 52 | 11.7 | 74 |
| **2** | Planar n–i–p | CuEtPc | $3.75 \times 10^{-4}$ | 1.01 | 22.81 | 49.9 | 11.5 | 74 |
| **3** | Planar n–i–p | CuPrPc | $2.16 \times 10^{-3}$ | 1.01 | 23.2 | 76.0 | 17.8 | 75 |
| **4** | Planar n–i–p | ZnPrPc | $1.948 \times 10^{-3}$ | 1.09 | 23.98 | 63.33 | 16.15 | 76 |
| **5** | Planar n–i–p | PdPrPc | $1.057 \times 10^{-3}$ | 1.07 | 23.81 | 71.04 | 18.09 | 76 |
| **6** | Mesoscopic | *n*-BuCuPc | $(5.0 \pm 0.6) \times 10^{-5}$ | 0.89 | 17.3 | 56 | 8.5 | 77 |
| **6** | Mesoscopic | *n*-BuCuPc | — | 1.04 | 20.9 | 66 | 14.4 | 78 |
| **6** | Mesoscopic | *n*-BuCuPc | — | 1.07 | 21.0 | 71 | 15.9 | 79 |
| **7** | Mesoscopic | *t*-BuCuPc | $(1.3 \pm 0.2) \times 10^{-6}$ | 0.94 | 13.8 | 43 | 5.6 | 77 |
| **7** | Mesoscopic | *t*-BuCuPc | — | 1.07 | 22.6 | 77.5 | 18.8 | 80 |
| **7** | Mesoscopic | *t*-BuCuPc | — | 1.13 | 23.19 | 71.3 | 18.68 | 81 |
| **2** | Planar n–i–p | CuEtPc | $20.4 \times 10^{-4}$ | 0.95 | 20.4 | 66.6 | 12.9 | 82 |
| **6** | Planar n–i–p | CuBuPc | $12.6 \times 10^{-4}$ | 1.02 | 21.0 | 50 | 15.0 | 82 |
| **8** | Planar n–i–p | CuHePc | $8.77 \times 10^{-4}$ | 0.97 | 17.4 | 68.1 | 11.5 | 82 |
| **9** | Mesoscopic | CuPc–TIPS | — | 1.01 | 21.4 | 65 | 14.0 | 83 |
| **10** | Mesoscopic | CuPc–OBu | $1.23 \times 10^{-4}$ | 1.06 | 22.8 | 73 | 17.6 | 84 |
| **11** | Mesoscopic | CuPc–Bu | $4.30 \times 10^{-4}$ | 1.03 | 21.0 | 66 | 14.3 | 84 |
| **12** | Planar n–i–p | OMe–DPA–CuPc | $1.55 \times 10^{-3}$ | 1.054 | 22.44 | 70.74 | 16.73 | 85 |
| **13** | Planar n–i–p | OMe–TPA–CuPc | $6.39 \times 10^{-3}$ | 1.096 | 23.41 | 76.67 | 19.67 | 85 |
| **14** | Planar n–i–p | SMe–TPA–CuPc | — | 1.132 | 24.10 | 84.31 | 23.00 | 53 |
| **15** | Mesoscopic | $ZnPcNO_2$–OPh | $2.80 \times 10^{-5}$ | 1.071 | 20.832 | 64.4 | 14.35 | 86 |
| **16** | Mesoscopic | $CuPcNO_2$–OPh | $1.86 \times 10^{-5}$ | 1.064 | 20.461 | 58.4 | 12.72 | 86 |
| **17** | Mesoscopic | $CoPcNO_2$–OPh | — | 1.04 | 11.79 | 64 | 8.24 | 87 |
| **18** | Mesoscopic | $CuPcNO_2$–OMFPh | $5.02 \times 10^{-5}$ | 1.02 | 20.01 | 60 | 12.52 | 88 |
| **19** | Mesoscopic | $CuPcNO_2$–OBFPh | $8.21 \times 10^{-5}$ | 1.04 | 20.62 | 64 | 13.66 | 88 |
| **20** | Mesoscopic | $ZnPcNO_2$–OBFPh | $11.4 \times 10^{-5}$ | 1.10 | 21.00 | 68 | 15.74 | 88 |
| **21** | Mesoscopic | ZnPc(*t*-Bu)$_4$ | — | 0.879 | 17.19 | 34.1 | 5.16 | 89 |
| **22** | Mesoscopic | (*n*-Bu)$_4$ZnPc | — | 0.928 | 14.5 | 61.8 | 9.00 | 90 |
| **23** | Mesoscopic | ZnPcAE | $66.10 \times 10^{-4}$ | 1.064 | 21.19 | 63.2 | 14.25 | 94 |
| **24** | Planar n–i–p | RE-$ZnBu_4Pc$ | $7.59 \times 10^{-4}$ | 0.94 | 21.83 | 63.10 | 12.94 | 91 |
| **25** | Planar n–i–p | $ZnBu_4Pc$ | $4.78 \times 10^{-4}$ | 0.95 | 20.74 | 69.64 | 12.06 | 91 |
| **26** | Mesoscopic | $H_2$-(*t*-Bu)$_4$Pc | — | 1.10 | 22.70 | 80.70 | 20.10 | 95 |
| **27** | Mesoscopic | OTPA–ZnPc | $1.08 \times 10^{-5}$ | 1.02 | 22.36 | 71.43 | 16.23 | 92 |
| **28** | Mesoscopic | ZnPH22 | $2.8 \times 10^{-4}$ | 1.06 | 22.5 | 77.0 | 18.3 | 96 |
| **29** | Mesoscopic | Methoxyethoxy-NiPc | $1.1 \times 10^{-6}$ | 1.13 | 23.92 | 78.66 | 21.23 | 50 |
| **30** | Mesoscopic | NiPc–Cou | $4.78 \times 10^{-6}$ | 1.061 | 19.50 | 49.4 | 10.23 | 93 |
| **31** | Mesoscopic | FePc–Cou | $3.65 \times 10^{-6}$ | 1.51 | 18.59 | 48.0 | 9.40 | 93 |
| **32** | Planar n–i–p | $CuMe_2Pc$ | $4.79 \times 10^{-2}$ | 1.085 | 21.32 | 68 | 15.73 | 97 |
| **33** | Planar n–i–p | $PdMe_2Pc$ | $3.42 \times 10^{-2}$ | 1.06 | 21.08 | 73 | 16.28 | 98 |
| **34** | Planar n–i–p | $HMe_2Pc$ | $2.72 \times 10^{-2}$ | 1.035 | 21.28 | 70.8 | 15.59 | 99 |
| **35** | Planar n–i–p | $ZnMe_2Pc$ | $1.80 \times 10^{-2}$ | 1.005 | 21.03 | 70.8 | 15.59 | 99 |
| **36** | Planar n–i–p | $Me_6Bu$–ZnPc | $6.85 \times 10^{-4}$ | 1.09 | 23.09 | 69.18 | 17.41 | 100 |
| **37** | Planar n–i–p | $NiEt_2Pc$ | $1.33 \times 10^{-5}$ | 0.96 | 18.65 | 48.32 | 8.63 | 101 |
| **38** | Planar n–i–p | $NiPr_2Pc$ | $3.64 \times 10^{-4}$ | 1.04 | 22.83 | 59.40 | 14.07 | 101 |
| **39** | Planar n–i–p | CuPc-$(OMe)_8$ | $1.1 \times 10^{-3}$ | 1.05 | 22.1 | 79 | 18.3 | 102 |
| **40** | Planar n–i–p | P-$SC_6$-TiOPc | $1.16 \times 10^{-5}$ | 0.95 | 19.92 | 36.04 | 6.82 | 103 |
| **41** | Planar n–i–p | NP-$SC_6$-TiOPc | $1.17 \times 10^{-4}$ | 1.06 | 22.31 | 71.34 | 16.87 | 103 |

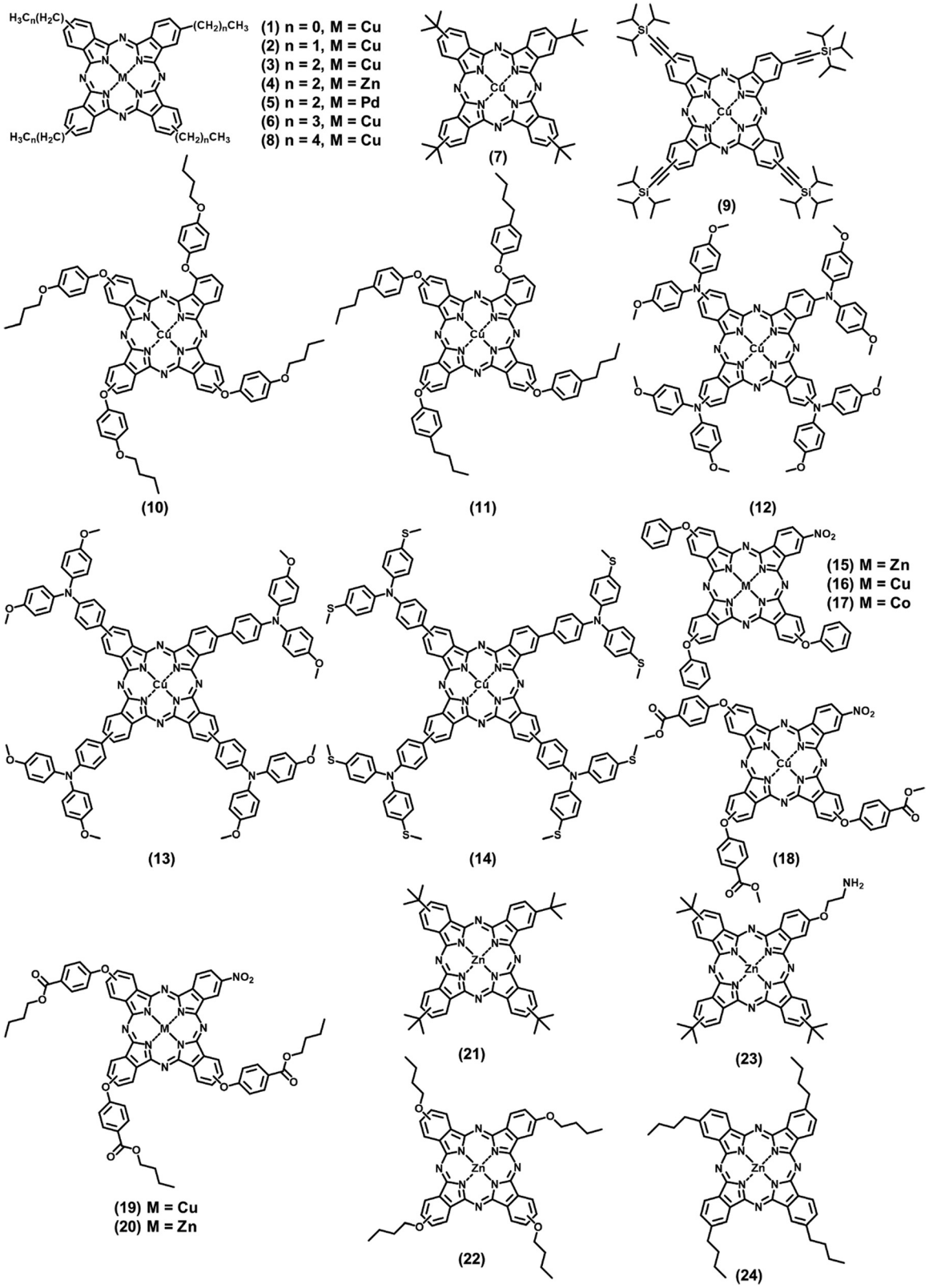


 

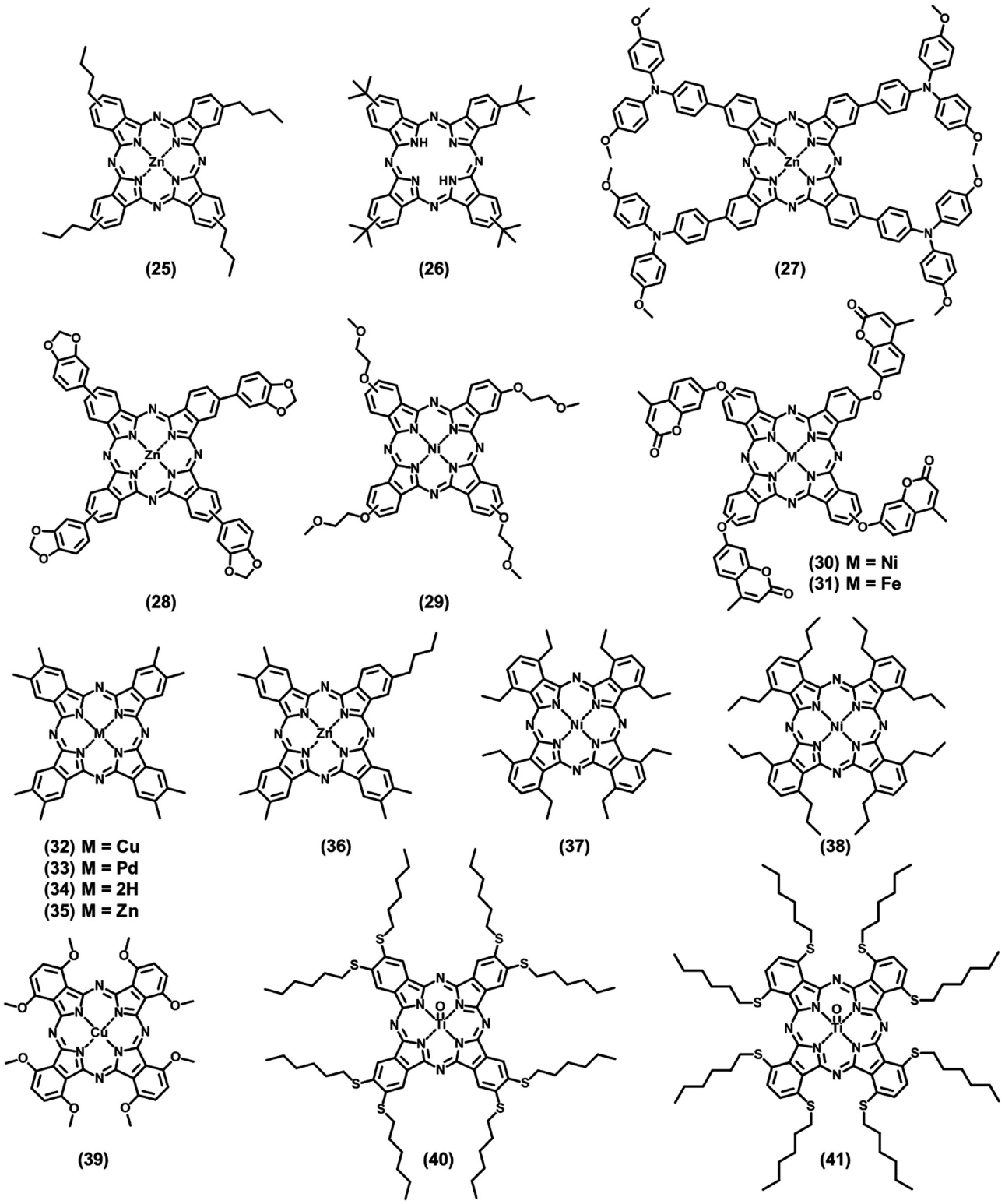


Fig. 3 Molecular structures of Pc-based dopant-free HTMs (**1–41**).

Therefore, substituting the Pd atom not only increased the LUMO level and band gap but also offered a longer carrier diffusion length. Due to the reduced hole electron recombination, a higher FF value was obtained for the PSCs using PdPrPc as the HTM, resulting in PCEs of up to 18.09%, with increased device stability.

Lianos and Xu's group added longer alkyl chains, such as *n*- and *tert*-butyl groups to the Pc ring (**6** and **7**) and investigated

their performance as HTMs in PSCs, respectively.[77] The long alkyl groups increased the molecular ordering and crystallinity of the Pc materials in the thin film samples. The higher crystallinity of the *n*-butyl-substituted CuPc (*n*-BuCuPc) was the origin of its higher hole mobility, which was almost 40 times higher than that of the *tert*-butyl-substituted CuPc material. Consequently, a better performance was observed for the perovskite devices based on tetra-*n*-butyl CuPc, with a PCE as high as 8.5%, compared with that of 5.6% for the PSCs employing *tert*-butyl-substituted CuPc as the dopant-free HTM. In another work, Lianos' group introduced a buffer layer of graphene oxide (GO) between *n*-BuCuPc as the HTM and the perovskite layer, which significantly improved the performance of their devices.[78] The presence of the buffer layer helped to reduce the shunt paths towards the electrode, offered higher stability to the perovskite layer, facilitated hole transfer, and reduced the charge recombination due to the improved HTM layer. Due to the mesoporous structure of GO, the extended aggregation and presence of voids in the Pc-based thin film were limited. Therefore, compared with the devices without a buffer layer, the PSCs using *n*-BuCuPc as the HTM and GO as the buffer layer in their structure showed enhanced FF and $V_{OC}$ values and a dramatic increase in PCE from 7.3% to 14.4%. A further increase in the cell efficiency was achieved when $TiO_2$/reduced GO was used as the ETM in a mesoscopic PSC instead of $TiO_2$, and a PCE of 15.9% was obtained.[79]

Kim and coworkers fabricated mesoscopic PSCs with high efficiency and thermal stability, utilizing tetra-*tert*-butyl-substituted CuPc (*t*-BuCuPc) as the HTM and a mixed perovskite of $(FAPbI_3)_{0.85}(MAPbBr_3)_{0.15}$ as the light absorbing material (Fig. 4a).[80] A virtually face-on orientation of *t*-BuCuPc was expected at the interface of the perovskite crystal facets, which was considered the main origin of the increase in both the charge transfer efficiency and long-term stability of the devices. The best-performing PSC achieved a PCE of 18.8%, with $V_{OC}$, $J_{SC}$, and FF values of 1.07 V, 22.6 mA $cm^{-2}$ and 77.5%, respectively. To investigate the long-term thermal stability of the devices, the *t*-BuCuPc-based PSC was kept on a hotplate at 85 °C for 1100 h inside a glovebox under an inert atmosphere. The device could maintain 97% of its initial efficiency for more than 1000 h of thermal annealing (Fig. 4b), which is particularly important, given that the operating temperature of the solar cells can easily become high under direct sunlight. Thus, the use of Pc materials in the device structure can be advantageous for PSCs working under high temperature. In 2018, Duong *et al.* used the soluble *t*-BuCuPc as the HTM in mesoscopic PSC devices and achieved PCEs as high as 20% through interfacial engineering.[81] It was observed that the solution-processed *t*-BuCuPc layer on top of the perovskite film possessed abundant cracks on its surface, which caused direct contact between the perovskite layer and the top electrode. Subsequently, heat treatment at 85 °C was applied to the devices, which resulted in negligible shunts and interface recombination (Fig. 4c). Interestingly, the cracks persisted on the CuPc film, even with the post heat treatment. However, it was verified that the Au particles on the contact rearranged after the heat treatment and migrated away from the cracks on the surface of the HTM layer. It is worth noting that only by using highly thermally stable Pc

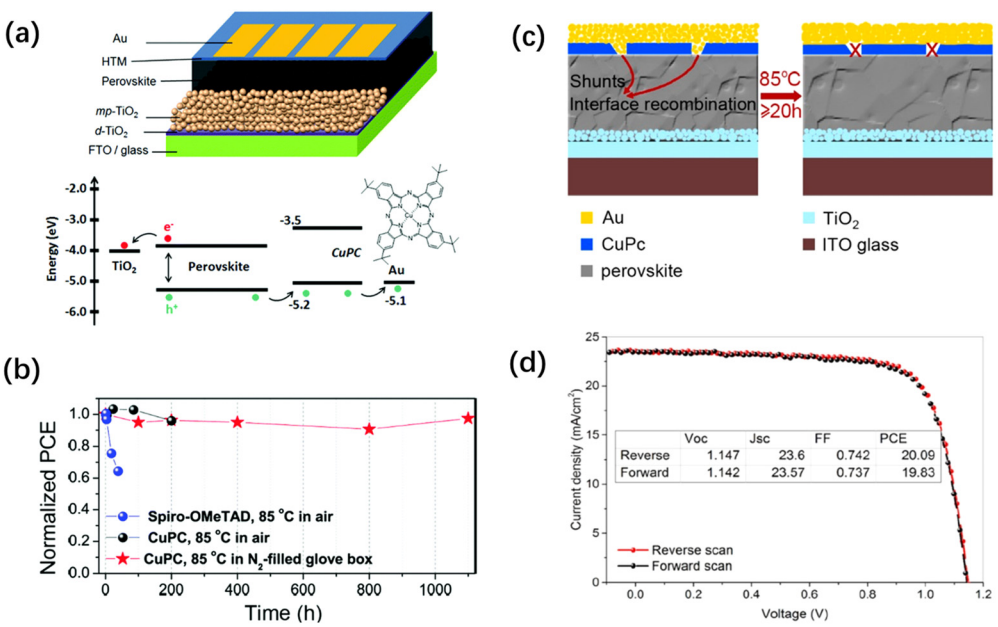


Fig. 4 (a) Schematic architecture of CuPc-applied perovskite solar cells (PSCs) and the energy-level diagram of the components used in these devices. (b) Long-term stability of the devices stressed at 85 °C in air (25–30% humidity), employing $FAPbI_3$/CuPc (black color) and $FAPbI_3$/spiro-OMeTAD (blue color). 1100 h stability of the device utilizing $FAPbI_3$/CuPc at 85 °C in a nitrogen-filled glove box (red color). Reproduced with permission.[80] Copyright 2017, RSC. (c) Schematic illustration of the impact of the post-heat treatment on the ion migration paths in the device structure. (d) *J*–*V* scans of the champion perovskite cell in both reverse and forward direction at a scan rate of 50 mV $s^{-1}$. The inset shows the photovoltaic parameters extracted from the *J*–*V* curves. Reproduced with permission.[81] Copyright 2018, ACS.

 

materials as the HTM in PSC devices structure it is possible to develop heating treatments for healing the device structure and enhancing its performance and operating lifetime. The *J–V* characteristics, together with the performance parameters of the champion device with the post heat treatment are presented in Fig. 4d, where negligible hysteresis can be observed for the device. In a recent study, our research group focused on the impact of the length of the alkyl group in peripherally tetra-substituted CuPc compounds when used as dopant-free HTMs on the PSC photovoltaic performance.[82] The results confirmed the role of the alkyl chain in the molecular orientation and intermolecular π–π stacking of Pc materials, and subsequently the hole mobility of their thin films. With an extended carbon chain length, improved crystallization was observed. Matching experimental data with calculations showed that alkyl-substituted CuPc materials have a tilted orientation on the perovskite layer with the angles of 46.56°, 39.58° and 34.00° for CuEtPc (**2**), CuBuPc (**6**), and CuHePc (**8**), respectively. Although the lower tilt angle of CuHePc was more beneficial for hole transport in the PSC, its greater π–π stacking distance suggested a weaker interaction, leading to lower hole mobility. The hole mobilities of CuEtPc, CuBuPc and CuHePc were measured by the SCLC method to be $20.4 \times 10^{-4}$, $12.6 \times 10^{-4}$ and $8.77 \times 10^{-4}$ $cm^2\ V^{-1}\ s^{-1}$, respectively. The CuBuPc-based PSCs exhibited a higher efficiency (15%) compared with the devices using CuEtPc (12.9%) and CuHePc HTMs (11.5%), which was attributed to the better morphology of the CuBuPc films on perovskite and their high hole mobility and more balanced charge transport.

Sun and coworkers introduced triisopropylsilylethynyl (TIPS) substituents in the periphery of the Pc ring to improve its solubility and hydrophobicity. CuPc–TIPS (**9**) was explored as an HTM in mesoscopic perovskite devices, in combination with mixed-ion perovskite materials and vacuum-free carbon counter electrode, resulting in a PCE of 14.0% under 1 Sun illumination intensity.[83] CuPc–TIPS showed significantly higher conductivity ($5 \times 10^{-6}$ S $cm^{-1}$) than pristine spiro-OMeTAD ($10^{-7}$–$10^{-8}$ S $cm^{-1}$).[83] In another work in 2019, the same team developed two dopant-free HTMs based on CuPc derivatives with non-peripheral substituents.[84] Their study confirmed that even small structural changes in the substituents could have a significant influence on the molecular ordering in thin films and the hole transport ability. The PSCs based on CuPc–OBu (**10**), with butoxy chains attached to phenoxy substituents, exhibited the best PCE of 17.6%, which was substantially higher than that of the devices employing the CuPc–Bu (**11**) HTM (14.3%), bearing butyl chains on the phenoxy groups. It was demonstrated that CuPc–OBu could offer higher hole mobility and more effective charge collection than CuPc–Bu due to the presence of extra oxygen molecules and higher flexibility of the C–O bond, and consequently a closer packing of the molecules. Recently, our research group achieved remarkable PCEs for PSCs using dopant-free HTMs based on arylamine-substituted CuPcs.[85] Methoxydiphenylamine-substituted copper phthalocyanine (OMe–DPA–CuPc, **12**) and methoxytriphenylamine-substituted copper phthalocyanine (OMe–TPA–CuPc, **13**) were employed as HTMs in planar n–i–p devices using $Cs_{0.05}(MA_{0.13}FA_{0.87})_{0.95}Pb(I_{0.87}Br_{0.13})_3$ as the light absorber and $SnO_2$ thin layer as the ETM, reaching efficiencies as high as 16.7% and 19.7%, respectively. According to the molecular dynamics (MD) simulation results, a higher density was calculated for OMe–DPA–CuPc (1.26 g $cm^{-3}$) with respect to OMe–TPA–CuPc (1.23 g $cm^{-3}$) in the bulk amorphous aggregates (Fig. 5a). Focusing on the intermolecular radial distribution function between the molecular centers of mass, short-range aggregation was obtained for OMe–TPA–CuPc compared to OMe–DPA–CuPc (Fig. 5b). In addition, the distribution of the intermolecular alignment of the nearest neighboring molecules revealed an orientation between about 80° to 85° for OMe–DPA–CuPc compared with the orientation values approaching 0° for the OMe–TPA–CuPc molecules, leading to more efficient π–π interactions for the latter (Fig. 5c). Due to the enhanced tendency of OMe–TPA–CuPc to form partially ordered aggregates, a larger mobility for OMe–TPA–CuPc can be expected with respect to OMe–DPA–CuPc. Accordingly, a higher hole mobility was measured by the SCLC method for OMe–TPA–CuPc ($6.39 \times 10^{-3}$ $cm^2\ V^{-1}\ s^{-1}$) than OMe–DPA–CuPc ($1.55 \times 10^{-3}$ $cm^2\ V^{-1}\ s^{-1}$). Moreover, the synthesis cost of OMe–TPA–CuPc was estimated to be 28.19 $ per g, which is much lower than that of spiro-OMeTAD. Moreover, in the aging test, the OMe–TPA–CuPc-based devices showed good stability, retaining 92% of their initial efficiency over 960 h (without encapsulation, in air, at 25 °C and under 75% humidity).

In a recent publication, the same research group explored the performance of methylthiotriphenylamine-substituted copper phthalocyanine (SMe–TPA–CuPc) (**14**) as a dopant-free HTM in PSCs with the n–i–p structure.[53] It was demonstrated that the SMe–TPA–CuPc molecules could diffuse into the perovskite film, effectively passivating the defects in the grain boundaries, as well as the surface of the film through the stronger interactions between the under-coordinated lead sites in the film and the methylthio moiety than the methoxy moiety of the Pc-based HTM (Fig. 5d and e). This holistic approach for passivating the perovskite layer resulted in an excellent performance and stability for the devices, delivering an incredible efficiency of 23.0%. This is among the highest efficiencies reported to date for PSC devices using dopant-free HTMs. After 3624 h of aging at 85 °C, the optimized PSCs could maintain 96% of their initial PCE. Guo *et al.* used asymmetric MPc materials as dopant-free HTMs in PSCs and reported PCEs of 12.72%, 14.35%, and 8.24% for the devices employing Cu-, Zn-, and Co-based HTMs, respectively.[86,87] With three phenoxy and a nitro substituent at the peripheral positions around the Pc ring, acting as ''push'' and ''pull'' groups, the developed Pc-based HTMs offered a donor–π–acceptor (D–π–A) structure, favoring their hole transport ability. Moreover, the flexible phenoxy groups enhanced the solubility of the MPc materials, as well as their molecular packing order. The improved performance of the $ZnPcNO_2$–OPh (**15**)-based PSCs was attributed to the higher hole mobility of $ZnPcNO_2$–OPh and its lower series resistance compared with $CuPcNO_2$–OPh (**16**) and $CoPcNO_2$–OPh (**17**). Guo and coworkers extended their research on $NO_2$-substituted asymmetric MPcs by introducing either (4-methylformate)phenoxy or (4-butylformate)phenoxy groups in the Pc macrocycle, using Cu and

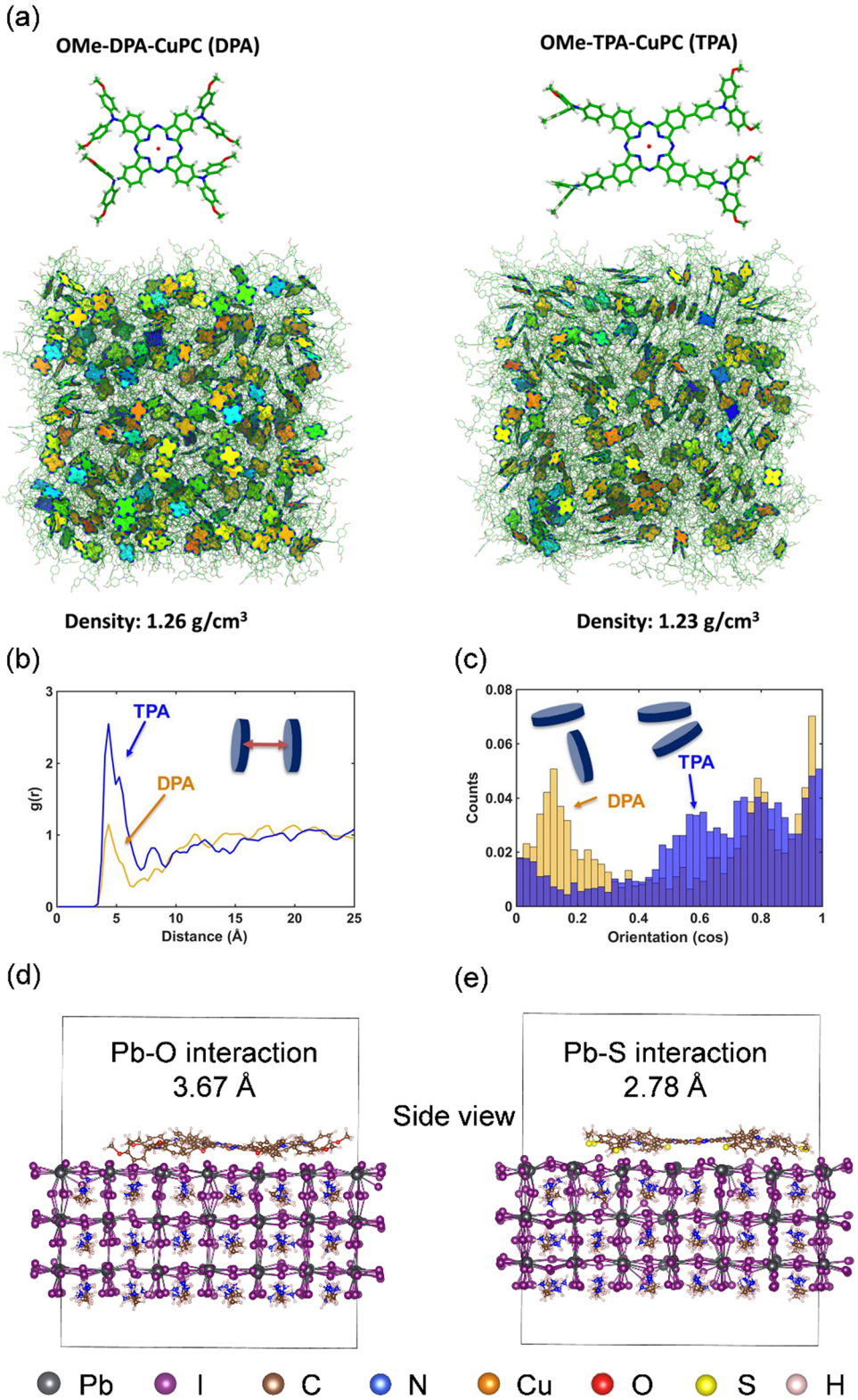


Fig. 5 (a) Molecular structure and simulated bulk aggregates (periodic cubic box, about 8 × 8 × 8 nm) of OMe–DPA–CuPc and OMe–TPA–CuPc. (b) Centers of mass and (c) distribution of the intermolecular alignment of nearest neighboring molecules (center of mass distance of <6.5 Å), defined as the angle between the normal to the planes of the two Pc cores. Adsorption structures equilibrated by AIMD simulation: side views of (d) OMe–TPA–CuPc/$MAPbI_3$ and (e) SMe–TPA–CuPc/$MAPbI_3$. Reproduced with permission.[85] Copyright 2019, Wiley.

 

Zn as metal centers.[88] Three novel dopant-free HTMs were developed and denoted as $CuPcNO_2$–OMFPh (**18**), $CuPcNO_2$–OBFPh (**19**), and $ZnPcNO_2$–OBFPh (**20**) and incorporated in mesoscopic PSCs. The higher hole mobility of $ZnPcNO_2$–OBFPh resulted in a higher $J_{SC}$ value and better performance for the cell in comparison to the PSCs utilizing the CuPc HTMs. The best-performing devices based on $ZnPcNO_2$–OBFPh presented a PCE of 15.74%, with $V_{OC}$, $J_{SC}$, and FF of 1.10 V, 21.00 mA $cm^{-2}$ and 68%, respectively. This study demonstrated the great potential of tetra-substituted ZnPc materials as HTMs in PSCs. In 2016, Wu *et al.* reported an efficiency of 5.16% and 7.98% under forward and reverse scans, respectively, for a mesoscopic perovskite device employing peripherally tetra-*tert*-butyl substituted ZnPc (**21**) as a dopant-free HTM.[89] Their device suffered from a very low FF and severe hysteresis, which is mainly due to the poor coverage of the perovskite layer on the mesoporous $TiO_2$ film. Similarly, Katz and coworkers observed considerable hysteresis in their PSC devices based on a tetra-*n*-butoxy-substituted ZnPc ($(n\text{-BuO})_4$ZnPc, **22**) HTM and achieved PCEs of 6.06% and 9.00% under forward and reverse scans, respectively.[90] Undesirable interfacial contact was considered the main origin of the observed hysteresis behavior in the devices. Consequently, by replacing one of the *tert*-butyl groups in tetra-substituted Zn and CuPc compounds, six asymmetric MPc materials were developed and used as dopant-free HTMs in PSC devices.[94] MPcs often possess a narrow band gap of 1.4 to 2.1 eV, which cause poor electron blocking and increased charge recombination at their interface with the perovskite film.[13] Thus, to overcome this problem, substituents are introduced in various positions around the Pc ring to tune the band gap of MPc materials. Additionally, through the appropriate selection of the substituents, the carrier diffusion length and the carrier mobility can be improved in the Pc thin film. Perturbing the electron conjugated system in the Pc ring by asymmetrically introducing different substituents will deliver a unique set of photophysical and electrochemical properties in the Pc compound. By investigating the charge carrier dynamics of the thin films of the developed MPcs *via* transient absorption spectroscopy (TAS), it was found that the charge carrier lifetime was synergically controlled by both the core metal and the different substitutes around the ring. Asymmetrically attached substituents around the Pc ring can impact the triplet state properties and deliver a longer lifetime for the generated charges. Eventually, the evaluation of the photovoltaic performance of the PSCs based on asymmetrical substituted ZnPcs indicated a jump in the efficiency of the asymmetric device (ZnPcAE (**23**)) with a PCE of 14.25% compared with that of the tetra-*tert*-Bu-substituted ZnPc (PCE = 10.52%).

Recently, we compared the performance of PSCs using either a pure isomer or isomer mixture of tetra-*n*-butyl-substituted ZnPc as a dopant-free HTM in their structure.[91] The use of pure isomer materials in the device structure as the active layers has been confirmed as an efficient approach to achieve a higher performance and lifetime in the devices.[104,105] It has been verified that various isomers of a Pc compound can offer different values of charge carrier mobility.[106] Accordingly, the use of a pure isomer Pc compound with the highest charge mobility and conductivity may endow the PSC device with a higher performance and stability. However, the common chromatography is not a suitable technique for separating and purifying various isomers of a Pc compound with four similar groups attached non-peripherally to the Pc ring. Therefore, a ring expansion method was used to synthesize the pure isomer ZnPc material (RE-$ZnBu_4$Pc, **24**). A considerably higher X-ray diffraction peak intensity was observed for RE-$ZnBu_4$Pc compared to ZnPc with the isomer mixture ($ZnBu_4$Pc, **25**), proving the greater tendency of the pure isomer compound to form films with higher crystallinity, which is advantageous for its charge carrier transport ability. The devices based on RE-$ZnBu_4$Pc showed a higher average performance with better reproducibility in the fabrication process, as well as better stability compared with the PSCs employing the isomer mixture Pc-based HTM ($ZnBu_4$Pc). The highest PCEs of 12.94% and 12.06% were achieved for the planar devices based on RE-$ZnBu_4$Pc and $ZnBu_4$Pc, respectively. The better film quality with higher crystallinity and higher hole mobility of RE-$ZnBu_4$Pc than $ZnBu_4$Pc were considered as the main reason for the better performance observed for the devices using this HTM material. The PSCs based on both pure isomer and mixture ZnPc materials showed good long-term stability after storage in an atmosphere with high relative humidity. In a study in 2021, the performance of tetra-*tert*-butyl-substituted metal-free Pc (**26**) as an HTM for n–i–p devices was explored, reporting efficiencies of over 20% for n–i–p devices, and compared to that of metal-Pc HTMs.[95] It is well-known that the pyrrolic nitrogen groups in the inner ring of the Pc molecule are highly reactive towards metal ions, and therefore can strongly interact with the under-coordinated $Pb^{2+}$ sites on the surface of the perovskite film and passivate its defects, further enhancing the $V_{OC}$ of the devices compared to their metal-coordinated counterparts. Cui and coworkers modified the performance of TPA-substituted ZnPc HTM by adding methoxy groups to the TPA moiety.[92] The methoxy groups endowed the ZnPc material with enhanced solubility in various organic solvents, leading to a more controlled thin film fabrication process using solution-based deposition techniques. The methoxy functional groups could also improve the interface between the perovskite and HTM layers and passivate the defects in the perovskite layer, leading to a better performance for the devices. OTPA–ZnPc (**27**) was used as a dopant-free HTM in PSC devices with a mesoporous $TiO_2$ ETM layer and mixed perovskite ($(FAPbI_3)_{0.85}(MAPbBr_3)_{0.15}$) absorber. OTPA–ZnPc showed a HOMO level of −5.58 eV, which is slightly higher than that of the mixed perovskite material (−5.65 eV), and its SCLC hole mobility was calculated to be $1.08 \times 10^{-5}$ $cm^2$ $V^{-1}$ $s^{-1}$. A smooth film of the HTM was uniformly formed on the top of the perovskite layer, inhibiting the direct contact between the perovskite layer and the electrode. The best-performing device exhibited a PCE as high as 16.23% under the reverse scan. In 2021, a series of ZnPc derivatives was synthesized bearing four phenyl-based substituents around the Pc scaffold and employed as dopant-free HTMs in n–i–p PSCs.[96] The device using the best-performing HTM, ZnPH22 (**28**), containing benzo[*d*][1,3]dioxole

peripheral substituents, could deliver a competitive PCE of 18.3%. It was suggested that the cyclic/planar conformation of ZnPH22, due to the unique structure of its peripheral groups, led to superior charge extraction and transport capability for the developed Pc-based HTM.

A series of Pc materials (CoPc, NiPc, ZnPc and $H_2Pc$) was designed using four methoxyethoxy units and employed in PSC devices as HTMs.[50] A record efficiency of 21.23% was achieved for a conventional n–i–p-structured PSC device based on the dopant-free tetra methoxyethoxy-substituted NiPc (**29**) (Fig. 6). It was demonstrated that among the used metal ions, Ni as the central atom could contribute more electrons to the Pc ring and construct a larger intramolecular electric field, which facilitated the interfacial charge extraction, improving the performance of the PSCs. In addition, the presence of two oxygen atoms in the methoxyethoxy substituents not only enhanced the molecular dipole, but also modified the dipole direction. The electron–hole pair density of four NiPc units can form a single connected flow manifold by intermolecular π orbitals, delivering efficient intermolecular charge transport (Fig. 6b). The high hole mobility of $1.1 \pm 0.2 \times 10^{-4}$ $cm^2\ V^{-1}\ s^{-1}$ was reported for the NiPc compound, which was considerably higher than that of CoPc ($8.8 \pm 0.3 \times 10^{-6}$ $cm^2\ V^{-1}\ s^{-1}$), ZnPc ($1.5 \pm 0.4 \times 10^{-5}$ $cm^2\ V^{-1}\ s^{-1}$), CuPc ($7.3 \pm 0.2 \times 10^{-5}$ $cm^2\ V^{-1}\ s^{-1}$) and $H_2Pc$ ($6.1 \pm 0.3 \times 10^{-5}$ $cm^2\ V^{-1}\ s^{-1}$).

By introducing four 7-coumarinoxy-4-methyl groups in the periphery of NiPc and FePc, Qi *et al.* developed new HTMs, which were denoted as NiPc–Cou (**30**) and FePc–Cou (**31**), respectively.[93] The coumarin groups facilitated a reduction in the aggregation of the Pc molecules and enhanced their solubility in organic solvents. PSCs with relatively good stability and PCEs of 10.23% and 9.40% were fabricated based on NiPc–Cou and FePc–Cou, respectively. NiPc–Cou showed a higher hole mobility ($4.78 \times 10^{-6}$ $cm^2\ V^{-1}\ s^{-1}$) compared with FePc–Cou ($3.65 \times 10^{-6}$ $cm^2\ V^{-1}\ s^{-1}$). With its HOMO level matched with that of perovskite layer and LUMO level higher than FePc–Cou, NiPc–Cou could offer greater hole extraction and conduction, as well as better electron blocking ability.

It was evidently established that the electronic nature and size of the substituents around the Pc macrocycle play a crucial role in defining the function of the Pc compound employed in PSC devices and its efficiency. A suitable substituent can adjust the solubility of the Pc materials in the appropriate solvents, and subsequently improve the quality of the deposited thin film by altering its morphology, crystallinity and thickness. By changing the electronic structure of the Pc compound, a substituent can help to match the energy levels of the frontier molecular orbitals in optoelectronic devices. Substituents can modify the intermolecular π–π stacking of the Pc core in the thin film, as well as the electrochemical properties of the Pc compounds, and consequently their performance as the active charge selective layer in the perovskite device. The bulkiness of the substituents can directly impact the aggregation of the Pc derivatives and their molecular arrangement and orientation inside the thin film, which successively influence their charge transport ability. Various substituents can also regulate the hydrophobicity of Pc compounds as an HTM layer in PSCs and improve the long-term stability of the devices.

**2.1.3. Octa-substituted Pc materials in PSCs.** Our research group studied peripherally substituted octamethyl Pc materials without and with different metal centers as dopant-free HTMs for PSCs, and considerable efficiencies have been achieved. Octamethyl-substituted Pcs are not soluble in common organic solvents, leading to the use of vacuum thermal evaporation for thin film deposition on the perovskite layer. In a study in 2017, the performances of PSC devices based on unsubstituted CuPc and $CuMe_2Pc$ (**32**) were investigated and compared.[97] The devices employing $CuMe_2Pc$ exhibited a 25% higher PCE and improved stability than that with CuPc. It was found that $CuMe_2Pc$ could form face-on molecular alignment on the perovskite surface, which resulted in high hole mobility, a dense thin film, and a surface with high hydrophobicity. The PSCs with a planar n–i–p structure and based on $CuMe_2Pc$ HTM achieved the highest PCE of 15.73%. Later, in another study, $PdMe_2Pc$ (**33**) was used as a dopant-free HTM in PSCs, and efficiencies as high as 16.28% were reported.[98] $PdMe_2Pc$ offered a high hole mobility of $3.42 \times 10^{-2}$ $cm^2\ V^{-1}\ s^{-1}$ and showed a long diffusion length (26.00 nm), thus limiting the charge recombination. Similar to $CuMe_2Pc$, $PdMe_2Pc$ could also

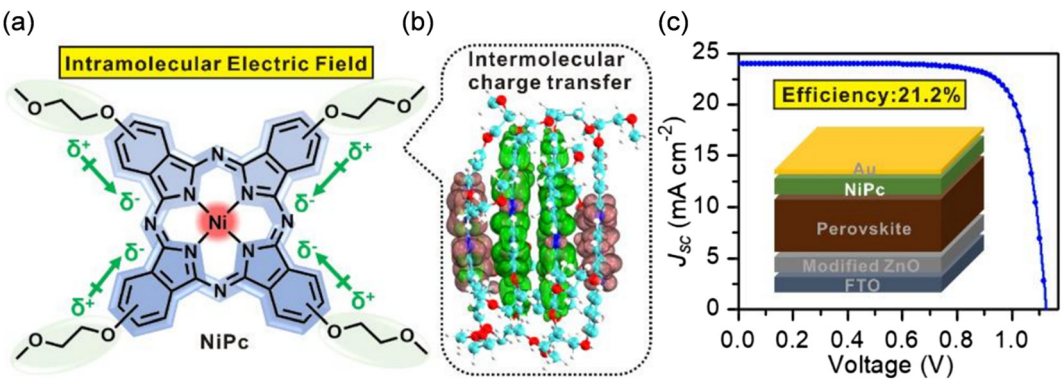


Fig. 6 (a) Structure of NiPc and direction of intramolecular electric field. (b) Hole–electron pair density isosurface (isovalue = 0.005 a.u.) in the simulated 4-periods NiPc structure unit. The pink and green isosurface represent electron and hole density, respectively. (c) *J–V* curve for the best-performing PSC with NiPc as HTM (Inset: Schematic illustration of the PSC with NiPc as HTM). Reproduced with permission.[85] Copyright 2019, Wiley.

 

adopt a face-on molecular alignment on the perovskite film. We continued our study on metal free ($HMe_2Pc$, **34**) and $ZnMe_2Pc$ (**35**) octamethyl-substituted Pc materials.[99] The PSC devices with an n–i–p planar architecture, employing an $SnO_2$ thin layer as the ETM, $CH_3NH_3PbI_3$ as the light absorbing layer and $HMe_2Pc$ and $ZnMe_2Pc$ as dopant-free HTMs, exhibited PCEs of 15.59% and 14.88%, respectively. Both HTMs showed suitable HOMO levels matched with the perovskite layer and Au electrode and high enough LUMO values to efficiently block the electrons. The GIXRD results confirmed the face-on molecular orientation of $HMe_2Pc$ and $ZnMe_2Pc$ when deposited on the perovskite layer. However, $HMe_2Pc$ exhibited a slightly higher hole mobility ($2.72 \times 10^{-2}$ $cm^2$ $V^{-1}$ $s^{-1}$) than $ZnMe_2Pc$ ($1.80 \times 10^{-2}$ $cm^2$ $V^{-1}$ $s^{-1}$), together with a better quenching ability, suggesting its higher efficiency to extract holes from the perovskite film and transfer them to the electrode. The grain size and morphology of both HTM thin films ($HMe_2Pc$ and $ZnMe_2Pc$) were very different. $HMe_2Pc$ exhibited particle-like grains with a smaller size than $ZnMe_2Pc$, which generated the grains with wire-like structures. Therefore, $ZnMe_2Pc$ formed a thin film with less coverage and more leakage on the perovskite, which was the origin of its worse performance compared with $HMe_2Pc$ HTM. Acknowledging the substantial role of the peripheral methyl substituents in adopting particular molecular positioning, we recently designed a new soluble ZnPc derivative with the capability of forming full face-on alignment on the perovskite layer.[100] Hexamethyl-mono-*n*-butyl-substituted ZnPc ($Me_6Bu$–ZnPc, **36**) was molecularly engineered and synthesized through a two-step ring expansion method. Although the presence of six methyl groups induced a full face-on molecular orientation, the higher solubility in common organic solvents was guaranteed by the *n*-butyl substituent. The developed HTM was applied in PSCs using a mixed perovskite ($Cs_{0.05}$-$(MA_{0.13}FA_{0.87})_{0.95}Pb(I_{0.87}Br_{0.13})_3$) light absorber. Interestingly, this face-on positioning was only available on the perovskite film due to the probable particular interactions between the methyl groups and different sites of the perovskite material on the surface (Fig. 7). The PSCs with $Me_6Bu$–ZnPc achieved PCEs of up to 17.41% and long-term stability and lost less than 10% of their efficiency after the 1400 h stability test at 25 °C and under a relative humidity of 75% without any encapsulation.

Continuing our research on octaalkyl-substituted MPc materials, we have recently reported the performance of PSCs employing dopant-free HTMs based on $NiEt_2Pc$ (**37**) and $NiPr_2Pc$ (**38**), with the alkyl groups attached to the non-peripheral positions around the Pc ring.[101] It was found that the length of the alkyl chain could play an important role in defining the energy level of the thin film. Due to the better alignment between the energy levels at the perovskite/HTL interface, $NiPr_2Pc$ with a longer alkyl chain could offer reduced charge recombination, and therefore higher $V_{OC}$ and $J_{SC}$ values for the device. The PSC based on $NiPr_2Pc$ could achieve the PCE of 14.07%. Recently, non-peripheral methoxy-substituted copper(II) phthalocyanine, denoted as CuPc-$(OMe)_8$, **39**, was investigated by the Cheng group.[102] The solution-processed CuPc-$(OMe)_8$ film exhibited comparable conductivity and hole mobility with the reference doped spiro-OMeTAD. Moreover, the as-prepared CuPc-$(OMe)_8$ showed better energy alignment with $(FAPbI_3)_{0.85}(MAPbBr_3)_{0.15}$ as a comparison of reference HTMs. The deposited uniform and compact CuPc-$(OMe)_8$ thin film could hinder the direct contact between the perovskite and top electrode layers. Consequently, the dopant-free CuPc-$(OMe)_8$-based PSCs showed a champion PCE of 18.3% accompanied with the $V_{OC}$, $J_{SC}$, and FF of 1.05 V, 22.1 mA $cm^{-2}$ and 79%, respectively. Recently, we developed two TiOPc derivatives, possessing eight *n*-hexylthio groups attached to either the peripheral (P-$SC_6$-TiOPc, **40**) or non-peripheral positions (NP-$SC_6$-TiOPc, **41**) of the Pc ring and applied them as dopant-free HTMs in

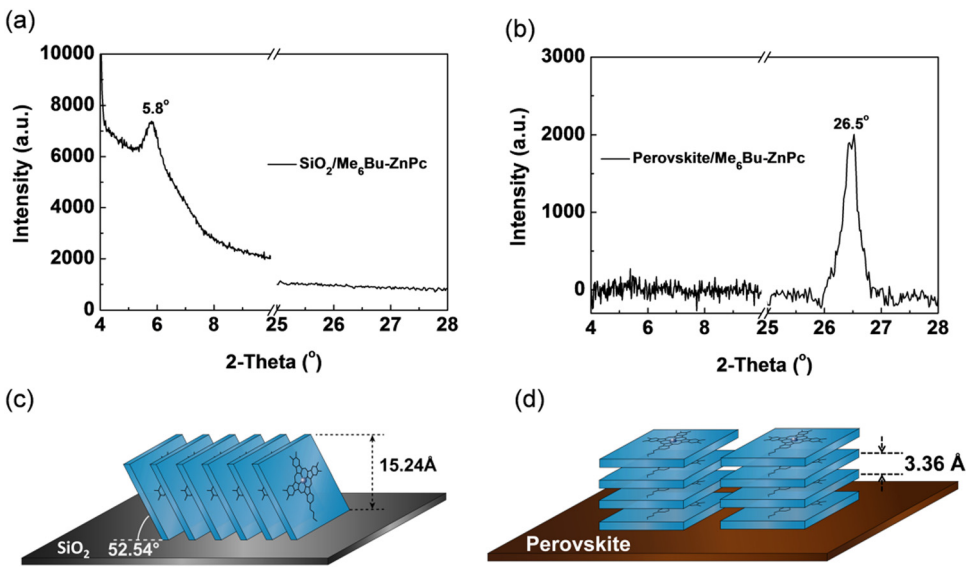


Fig. 7 GIXRD patterns of $Me_6Bu$–ZnPc deposited on (a) $SiO_2$ and (b) perovskite (thin film thickness of ~60 nm). Molecular orientation model of $Me_6Bu$–ZnPc deposited on (c) $SiO_2$ and (d) perovskite. Reproduced with permission.[100] Copyright 2019, Wiley.

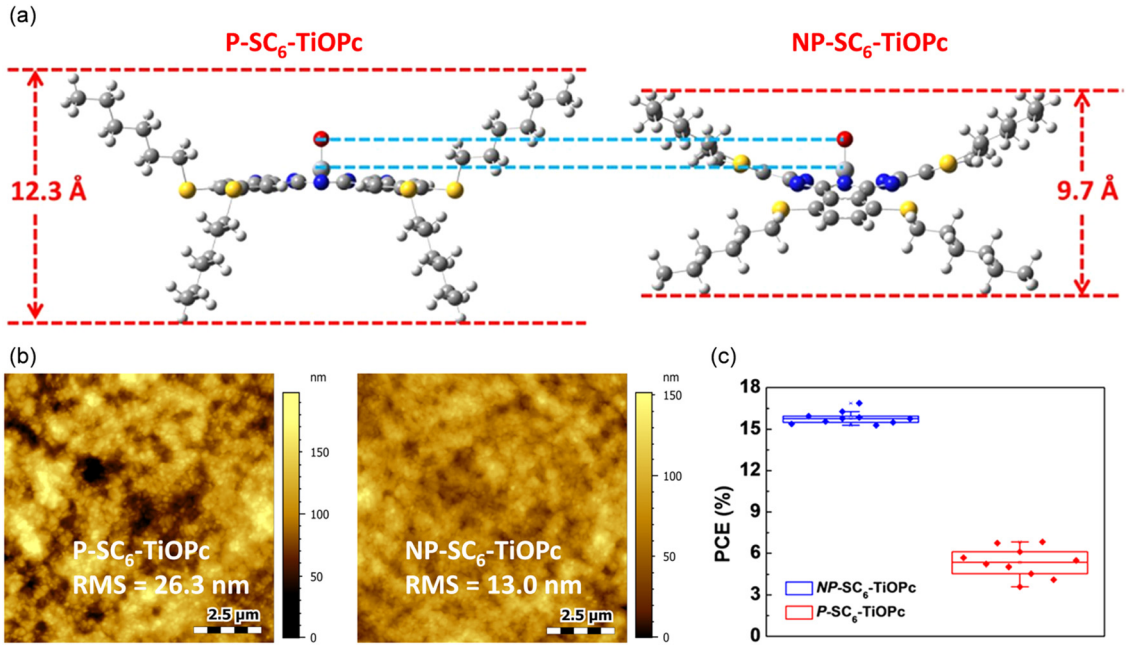


Fig. 8 (a) DFT results of the side view of the P-$SC_6$-TiOPc- and NP-$SC_6$-TiOPc-optimized ground state geometry (Gaussian 09 optimization with DFT B3LYP/6-31g(d)). (b) AFM images of P-$SC_6$-TiOPc deposited and NP-$SC_6$-TiOPc deposited on perovskite. (c) PCE statistics of devices fabricated from the same batch. Reproduced with permission.[103] Copyright 2019, ACS.

planar n–i–p PSCs.[103] According to density functional theory (DFT) calculation results, a larger rotation angle for the substituents on the peripheral, compared with non-peripheral positions, led to an increased height for the P-$SC_6$-TiOPc compound, and consequently a greater distance and weaker π–π interactions between the molecules in the P-$SC_6$-TiOPc thin film (Fig. 8a). Therefore, significantly higher hole extraction and mobility were obtained for NP-$SC_6$-TiOPc than the P-$SC_6$-TiOPc thin film. Furthermore, the different sizes and intermolecular interactions of the P-$SC_6$-TiOPc and NP-$SC_6$-TiOPc compounds resulted in some alterations in their thin film morphology. A thin film with an improved morphology, lower surface roughness, and better coverage on the perovskite layer was achieved for NP-$SC_6$-TiOPc compared with P-$SC_6$-TiOPc (Fig. 8b). The PSCs using NP-$SC_6$-TiOPc achieved the highest PCE of 16.87%, which was remarkably higher than that of P-$SC_6$-TiOPc-based devices (6.82%). It was demonstrated that tuning the position of the attached substituents can be considered as an effective strategy to enhance the performance of Pc-based PSC devices. Significantly higher reproducibility was achieved for the devices based on NP-$SC_6$-TiOPc as a dopant-free HTM due to its higher ordering and higher-quality thin film (Fig. 8c). The photovoltaic properties of some selected perovskite devices using octa-substituted Pc compounds in their structure are summarized in Table 2.[50,93,97–103]

### 2.2. Doped phthalocyanines for PSCs

The introduction of a bulky group at the peripheral sites of the Pc core may suppress the aggregation and reduce the π–π interaction.[14] However, it also results in low hole mobility and conductivity, which are unfavorable for efficient hole transport in devices. Accordingly, a common method to overcome this issue is the doping strategy. As a successful approach in the case of spiro-OMeTAD, doping with bis(trifluoromethylsulphonyl)imide (Li-TFSI), 4-*tert*-butylpyridine (*t*BP) and tri(bis(trifluoromethane)sulfonimide) (FK209) led to a reduction in the spiro-OMeTAD molecule LUMO level. Accordingly, the energy gap between the pristine spiro-OMeTAD and the radical cation species provides the driving force for charge hopping between these two materials, significantly improving the conductivity and mobility in the doped form.[107] Considering this, doping was utilized in Pc HTMs to improve the performance of PSCs. The molecular structures of the Pc materials used as doped HTMs in PSCs are shown in Fig. 9 (**42–65**).

In 2015, Nazeeruddin's group explored the performance of Zn(II)octa(2,6-diphenylphenoxy)phthalocyanine (TT80, **42**) as a doped HTM in PSCs and reported a PCE of 6.7% under AM1.5G standard conditions.[108] The introduction of eight bulky substituents in the peripheral sites around the Pc ring led to the suppression of aggregation and a significant increase in the solubility of the ZnPc material, allowing the use of solution-processed deposition techniques. The same research group further introduced different secondary amine substituents in the periphery of the ZnPc ring to develop new HTMs for perovskite devices.[109] The PSCs using the newly synthesized HTMs, denoted as BI25 (**43**), BL07 (**44**), and BL08 (**45**), achieved the PCEs of 11.75%, 6.65%, and 11.44%, respectively. In 2019, they developed a series of octa-substituted MPcs with eight secondary aromatic amines bound to the peripheral positions of the macrocycle by C–N bonds, which were denoted as BL25 (**46**), BL38 (**47**), BL40 (**48**), BL50 (**49**), BL51 (**50**) and BL52 (**51**).[110] The results showed that the MPcs featuring bis(*p*-alkoxyphenyl)amino substituents delivered a better photovoltaic

 

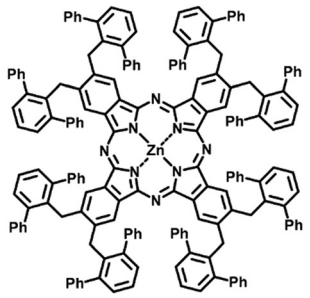


(42)

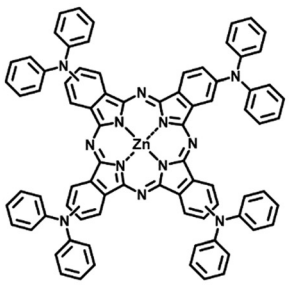


(43)

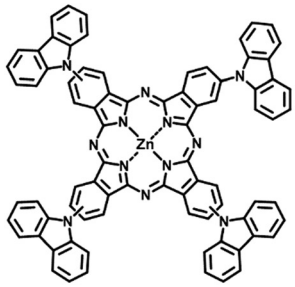


(44)

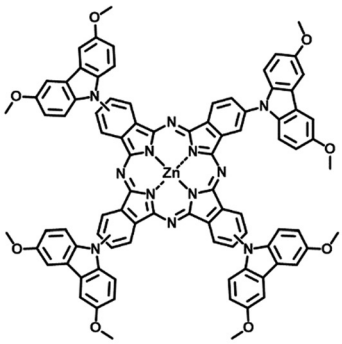


(45)

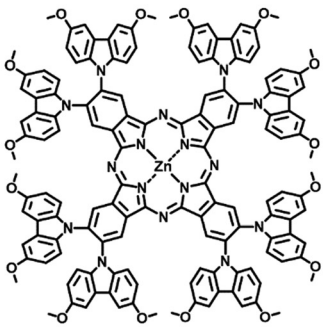


(46)

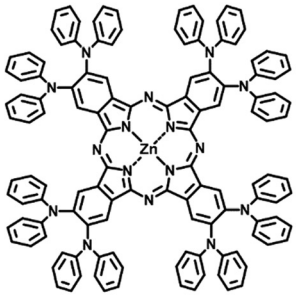


(47)

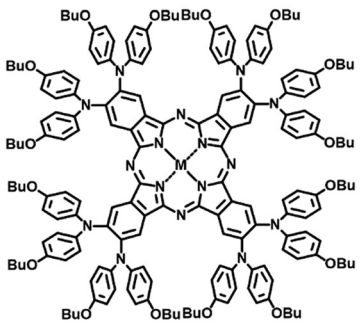


(48) M = Zn
(49) M = Cu

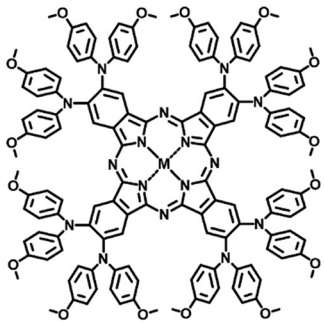


(50) M = Zn
(51) M = Cu

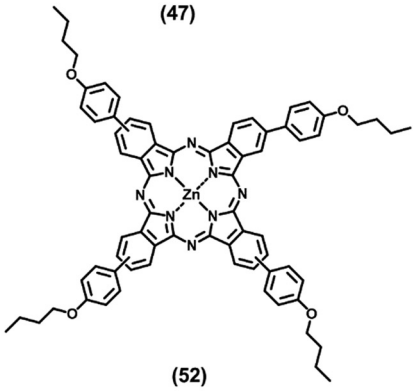


(52)

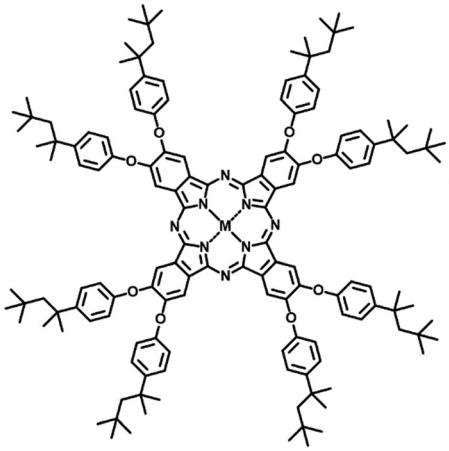


(53) M = Cu
(54) M = Zn

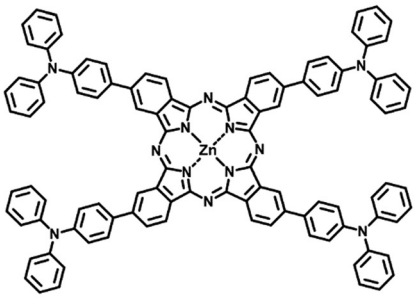


(55)

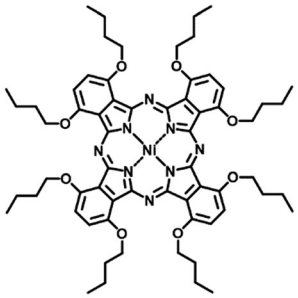


(56)

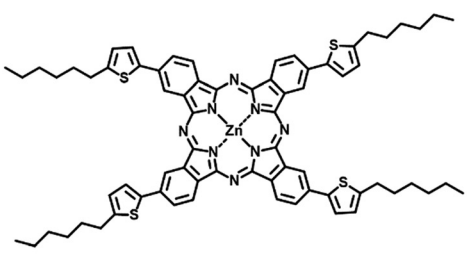

(57)

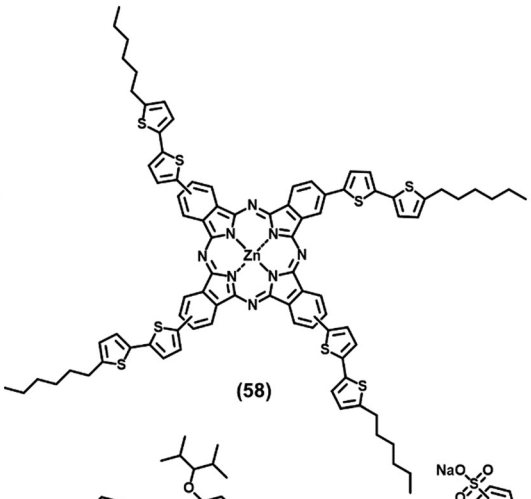

(58)

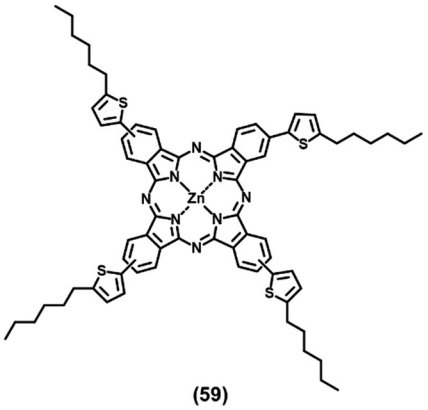

(59)

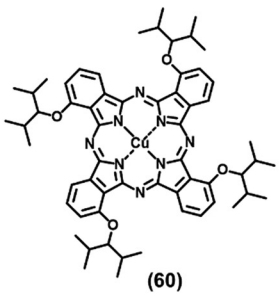

(60)

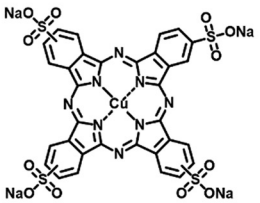

(61)

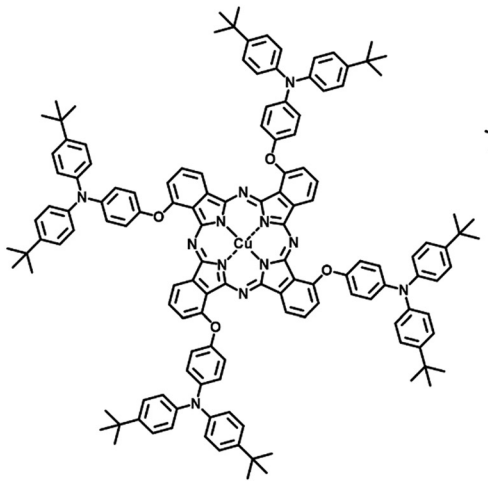

(62)

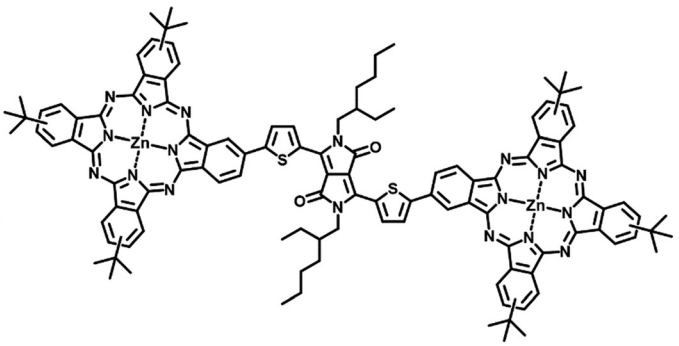

(63)

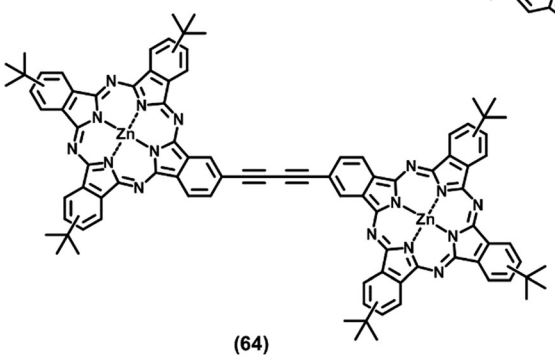

(64)

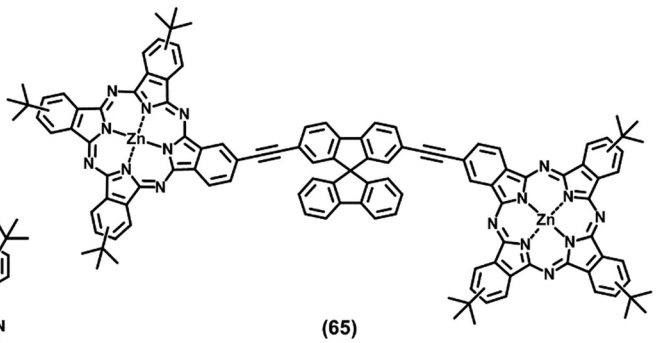

(65)

 

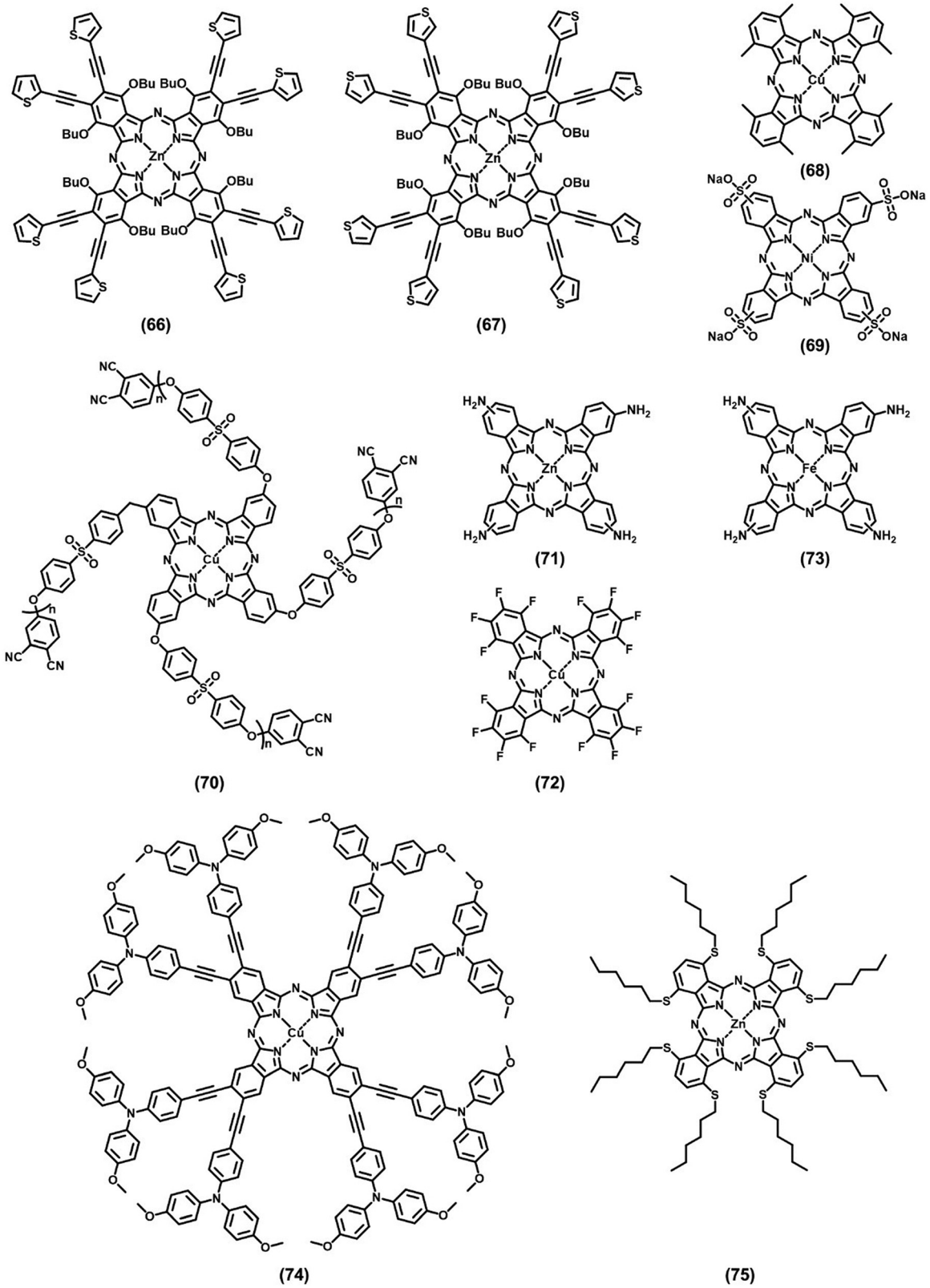


Fig. 9 Molecular structures of Pc as doped HTMs (**42–65**) and additive in HTM or perovskite layer in PSCs (**66–75**).

performance than their 9*H*-carbazol-9-yl and diphenylamino analogs, and the core metal in the Pc derivatives with the same structure had little effect on their overall performances. A superior PCE of up to 18.10% was achieved by the HTM of

ZnPc bearing eight bis(*p*-butoxyphenyl)amino substituents (BL40), which is comparable to that of spiro-OMeTAD with dopants (19.25%). The explanation for the huge gap in the PCE between BL25 and BL38 with the remaining ones was investigated by PL decay kinetics, electric field dependent time-resolved photoluminescence experiments, and photocurrent kinetics upon photoexcitation of the device with short nanosecond laser pulses, indicating that the former two types of HTMs have large nonradiative surface recombination and an injection barrier for holes. In a recent study by the same group, efficiencies of around 20% were reported by the same team, using a newly synthesized HTM from the same family named Zn-BL54 (**52**) with tetra-substituted Pc ring, and double or triple cation perovskite materials as the light-absorbing film in the device.[111] The achieved efficiencies were comparable with that of the reference devices using spiro-OMeTAD, while offering considerably higher long-term stability for the non-encapsulated devices. In 2017, Calio and coworkers altered the diphenyl groups attached to the phenoxy by *tert*-octyl, and developed two new Pc materials substituted by 4-*tert*-octylphenol groups, with Cu(II) and Zn(II) as the metal center, which were denoted as ($^t$OctPhO)$_8$CuPc (**53**) and ($^t$OctPhO)$_8$ZnPc (**54**), respectively.[112] The MPc-based HTMs were doped by adding lithium LiTFSI and (tBP) and tested in PSCs with mixed perovskites ((FAPbBr$_3$)$_{0.85}$(MAPbI$_3$)$_{0.15}$), and the thickness of their thin layers was optimized. It was demonstrated that a thinner layer of either HTM could offer a lower series resistance, and consequently an improved performance for the devices. The best-performing devices based on ($^t$OctPhO)$_8$CuPc and ($^t$OctPhO)$_8$ZnPc exhibited PCEs of 8.33% and 7.25%, respectively. In their study, the Lianos' group employed tetraphenylamine-substituted ZnPc (TPA-ZnPc, **55**) as an HTM doped with tBP and LiTFSI in PSCs, reaching an efficiency of 9.0%, which was further enhanced to 13.65% in the presence of an $Al_2O_3$ buffer layer between the perovskite and HTM layers.[113] The presence of the buffer layer offered a higher shunt resistance in the device, as well as higher stability for the perovskite layer, protecting it against the corrosive additives used in the HTM. Moreover, the porous framework of $Al_2O_3$ facilitated the formation of a thin film as the upper HTM layer, leading to better hole transfer and conduction and limited charge recombination. According to the cross-sectional FESEM image, a thicker hole transporting layer was achieved on the top of the $Al_2O_3$ buffer layer compared with neat TPA-ZnPc. The performance of the device was enhanced with the optimum thickness of 200 nm for the buffer and HTM layers combined.

Sun's group introduced eight butoxy groups in the non-peripheral sites around the NiPc macrocycle (NiPc–(OBu)$_8$, **56**), and in combination with vanadium(V) oxide ($V_2O_5$), developed an organic–inorganic integrated hole transport layer for incorporation in mesoscopic PSC devices.[114] The PSCs based on pristine NiPc–(OBu)$_8$ exhibited efficiencies of up to 10.6%, while doping NiPc–(OBu)$_8$ with LiTFSI and tBP, together with an increase in its thin film thickness could significantly enhance the PCEs of the devices to 17.9%. Although the pristine NiPc–(OBu)$_8$ showed lower conductivity ($1.18 \times 10^{-4}$ S cm$^{-1}$) than the doped spiro-OMeTAD ($1.91 \times 10^{-4}$ S cm$^{-1}$), the doping strategy could considerably enhance its conductivity to a value of $1.97 \times 10^{-4}$ S cm$^{-1}$. The use of a $V_2O_5$ buffer layer on top of the dopant-free NiPc–(OBu)$_8$ film led to the highest efficiency of 18.3% for the devices. A PCE of 10.8% was achieved for the PSCs with only a $V_2O_5$ HTM, confirming the critical role of the organic–inorganic HTM in achieving high efficiencies. The integrated HTM could fully cover the perovskite crystals and lower the recombination losses between the perovskite and Au electrode. Nazeeruddin's group introduced thiophene-based functional groups in the ZnPc ring and studied their performance as an HTM in perovskite devices.[115] Using a hybrid interfacial hole transport layer, consisting of a tetra 5-hexyl-2-thiophene-substituted ZnPc (Sym-HTPcH, **57**) HTM and *meso*-$Al_2O_3$ buffer layer, devices with efficiencies of up to 12.8% were achieved.[115] The device performance has been considerably improved by changing the thiophene-based functional groups around the ZnPc ring.[116] Tetra-5-hexyl-2,2′-bisthiophene-substituted ZnPc (HBT-ZnPc, **58**) and tetra-5-hexylthiophene-substituted ZnPc (HT-ZnPc, **59**) were employed in mesoscopic PSCs with (FAPbI$_3$)$_{0.85}$(MAPbBr$_3$)$_{0.15}$ perovskite absorber, showing the remarkable efficiencies of 15.5% and 17.5%, respectively. The higher efficiency of the HT-ZnPc-based PSCs was attributed to the enhanced molecular packing order of HT-ZnPc. Sun's group studied non-peripherally substituted CuPc materials by incorporating four 2,4-dimethyl-3-pentoxy groups in the CuPc ring and used as them as the HTM in mesoscopic PSCs based on (FAPbI$_3$)$_{0.85}$(MAPbBr$_3$)$_{0.15}$ light absorber and CuPc-DMP (**60**) HTM doped with LiTFSI and tBP, achieving PCEs of up to 17.1%.[117]

Tetrafluorotetracyanoquinodimethane ($F_4$-TCNQ) as a p-type doping material has attracted significant attention because of its strong electron affinity.[118–121] The prerequisite for molecular doping is that the electron affinity of the dopant is in the range of the ionization energy of the HTM. The extra mobile holes induced by the p-type dopant boost the charge carrier density in the HTM, leading to higher conductivity.[45] Therefore, the selection of a Pc with a suitable HOMO value matching the LUMO of $F_4$-TCNQ is feasible to realize a charge–transfer reaction between Pc and the dopant. Liao's group employed TS-CuPc doped with $F_4$-TCNQ in planar PSCs with normal and inverted architectures.[122] The addition of 2.5 wt% of $F_4$-TCNQ to the Pc material considerably enhanced the hole mobility of the thin film from $2.3 \times 10^{-4}$ to $9.2 \times 10^{-3}$ cm$^2$ V$^{-1}$ s$^{-1}$. In addition, an aqueous solution of TS-CuPc (**61**) with $F_4$-TCNQ showed a pH value of 7.4, which favored the long-term stability of the devices. The use of the doped TS-CuPc as the HTM in an inverted PSC led to a PCE of 16.14% compared to the reference device based on PEDOT:PSS, with the highest efficiency of 13.22%. TS-CuPc:$F_4$-TCNQ was also used as a hole modification layer between spiro-OMeTAD as the HTM and Ag electrode in n–i–p devices, which increased the efficiency of the PSCs from 16.23% to 20.16%. $F_4$-TCNQ was also employed by Sun's research group as a dopant for non-peripherally substituted tetra-4-(bis(4-*tert*-butyl)phenyl)amino)phenoxy copper phthalocyanine (CuPc-OTPA$^t$Bu, **62**) HTM in PSCs.[123] As a well-known electron donor, four triphenylamine (TPA) groups were introduced in the CuPc ring *via* oxygen atoms. The attached *tert*-butyl chains

 

Table 3 Photovoltaic properties of some selected perovskite devices employing doped Pcs in their structure

| Chemical structure no. | Device architecture | HTM | Hole mobility of HTM ($cm^2\ V^{-1}\ s^{-1}$) | $V_{OC}$ (V) | $J_{SC}$ (mA $cm^{-2}$) | FF (%) | PCE (%) | Ref. |
|---|---|---|---|---|---|---|---|---|
| **42** | Mesoscopic | TT80 | | 0.80 | 16.35 | 50.3 | 6.7 | 108 |
| **43** | Mesoscopic | BI25 | | 1.014 | 16.67 | 68.1 | 11.75 | 109 |
| **44** | Mesoscopic | BL07 | | 1.001 | 10.69 | 59.8 | 6.65 | 109 |
| **45** | Mesoscopic | BL08 | | 1.034 | 17.43 | 61.0 | 11.44 | 109 |
| **46** | Mesoscopic | BL25 | | 0.69 | 20.07 | 35.7 | 4.93 | 110 |
| **47** | Mesoscopic | BL38 | | 0.89 | 21.46 | 56.8 | 10.89 | 110 |
| **48** | Mesoscopic | BL40 | | 1.07 | 22.92 | 73.5 | 18.10 | 110 |
| **49** | Mesoscopic | BL50 | | 1.06 | 22.52 | 74.2 | 17.81 | 110 |
| **50** | Mesoscopic | BL51 | | 1.04 | 22.58 | 69.4 | 16.25 | 110 |
| **51** | Mesoscopic | BL52 | | 1.04 | 22.54 | 70.3 | 16.46 | 110 |
| **52** | Mesoscopic | Zn-BL54 | | 1.07 | 23.87 | 79.0 | 20.18[a] | 111 |
| **52** | Mesoscopic | Zn-BL54 | | 1.081 | 23.73 | 78.0 | 20.00[b] | 111 |
| **53** | Mesoscopic | $(^t$OctPhO$)_8$CuPc | | 0.87 | 19.01 | 50.56 | 8.33 | 112 |
| **54** | Mesoscopic | $(^t$OctPhO$)_8$ZnPc | | 0.89 | 17.52 | 46.52 | 7.25 | 112 |
| **55** | Mesoscopic | TPA-ZnPc | | 0.95 | 20 | 72 | 13.65 | 113 |
| **56** | Mesoscopic | NiPc–$(OBu)_8$ | | 1.070 | 23.0 | 72.8 | 17.9 | 114 |
| **56** | Mesoscopic | NiPc–$(OBu)_8$ | $1.90 \times 10^{-4}$ | 0.895 | 18.5 | 63.8 | 10.6 | 114 |
| **56** | Mesoscopic | NiPc–$(OBu)_8/V_2O_5$ | | 1.080 | 23.1 | 73.4 | 18.3 | 114 |
| **57** | Mesoscopic | Sym-HTPcH | | 0.988 | 17.2 | 74 | 12.8 | 115 |
| **58** | Mesoscopic | HBT-ZnPc | | 1.10 | 20.16 | 69.4 | 15.5 | 116 |
| **59** | Mesoscopic | HT-ZnPc | | 1.05 | 20.28 | 80.3 | 17.1 | 116 |
| **60** | Mesoscopic | CuPc-DMP | | 1.04 | 23.2 | 71 | 17.1 | 117 |
| **61** | Planar n–i–p | spiro-OMeTAD/ TS-CuPc: $F_4$-TCNQ | $9.2 \times 10^{-3}$ | 1.12 | 24.32 | 74 | 20.16 | 125 |
| **61** | Planar p–i–n | TS-CuPc:$F_4$-TCNQ | $9.2 \times 10^{-3}$ | 0.96 | 21.71 | 77 | 16.14 | 125 |
| **62** | Mesoscopic | CuPc-OTPA$^t$Bu:$F_4$-TCNQ | | 1.01 | 21.9 | 68 | 15.0 | 123 |
| **63** | Mesoscopic | ZnPc 1 | $2.83 \times 10^{-5}$ | 1.03 | 23.21 | 68.9 | 16.49 | 124 |
| **64** | Mesoscopic | ZnPc 2 | $1.50 \times 10^{-5}$ | 1.04 | 22.25 | 55.3 | 12.82 | 124 |
| **65** | Mesoscopic | ZnPc 3 | $4.08 \times 10^{-5}$ | 1.04 | 23.63 | 74.6 | 18.32 | 124 |

[a] Refers to the device with double cation perovskite and. [b] Refers to the device with triple cation perovskite.

also enhanced the solubility of the molecularly engineered HTM in common organic solvents and improved the hydrophobicity of its thin film. When 6 wt% of dopant was added to the HTM, the bulk conductivity of the HTM significantly increased, leading to an efficiency of 15.0% for the mesoscopic devices, which is comparable to the reference devices based on spiro-OMeTAD doped with LiTFSI and tBP(highest PCE of 15.3%).

Linking two or more Pc compounds can expand their π delocalization system and enhance their charge mobility. Although an expanded 2D planar structure for Pc materials can increase the risk of achieving rough and thick films with low coverage due to the formation of extensive crystalline domains, well-designed 3D structures can deliver more uniform films given that they have less intense intermolecular interactions. In 2022, three ZnPc dimers were developed as HTMs in perovskite devices.[124] In their structures, three different linkers, *i.e.*, diketopyrrolopyrrole (DPP) (ZnPc 1 (**63**)), two contiguous triple bonds (ZnPc 2 (**64**)), and spirobifluorene (ZnPc 3 (**65**)), were used to endow the designed HTMs with a wider range of electronic and structural properties. The PC dimers were doped with *t*BP and LiTFSI and employed in n–i–p-structured PSCs. The PCE of the devices using ZnPc 1, ZnPc 2 and ZnPc 3 were 16.49%, 12.82% and 18.32%, respectively, compared to the reference device based on doped spiro-OMeTAD with the PCE of 17.42%. The lower performance of ZnPc 1 and ZnPc 2 was attributed to their lower solubility or higher molecular aggregation. The photovoltaic properties of some selected perovskite devices using doped Pc compounds as the HTM layer are summarized in Table 3.[108–117,122–124]

### 2.3. Phthalocyanines as hole modification layer in PSCs

Dai's group introduced the insertion of a ZnPc hydrophobic hole modification layer between the light harvesting layer and doped spiro-OMeTAD to address the instability issue of PSCs.[69] The Bilayer HTM-based PSC with Nb-doped $TiO_x$ as the ETM exhibited an improved PCE of 16.8% compared to 15.1% for the unmodified HTM devices. With the introduction of the ZnPc modification layer, the series resistance ($R_s$) slightly increased, while the interface resistance of the HTM/absorber ($R_{HTM}$) and the total resistance ($R_s + R_{HTM}$) showed the opposite trend, indicating that the addition of the interfacial buffer layer reduced the charge recombination and resulted in lower resistive voltage loss, current loss and higher PCE. Because of the hydrophobic properties of the ZnPc, the modified devices retained 91% of the initial PCE after 2400 h in an ambient environment without encapsulation. In 2022, our research group employed two thiophene-functionalized metal-free Pc isomers, Pc S2 (**66**) and Pc S3 (**67**), as the passivating agent for the $MAPbI_3$ perovskite in an n–i–p-structured device.[52] The Pc materials were added to the perovskite layer by dissolving in an anti-solvent, allowing them to impact the perovskite crystal growth mechanism. Using DFT calculations, the interaction between the S atoms in the structure of the developed Pc compounds and the under-coordinated $Pb^{2+}$ was predicted.

The Pc molecules not only passivate the bulk defect, but also form a rigid thin film layer on the perovskite surface for surface defect passivation. The introduction of the Pc materials in the perovskite layer helped improve the grain size by slowing down the crystallization step during the formation of the thin film and drying process. However, the S atoms were located at different positions in the two Pc materials, resulting in different affinities toward the perovskite material. This led to a higher quality for the Pc S3-added perovskite film and an efficiency as high as 18% for the fabricated PSC based on the same material. The maximum PCE obtained for the PSCs based on $MAPbI_3$ without Pc and Pc S2-added perovskite was 16.88% and 16.64%, respectively. Additionally, the passivated devices showed a significant improvement in their moisture and thermal stability.

### 2.4. Phthalocyanines as additives in HTMs

The introduction of a p-type dopant in the HTM is an effective method to strengthen the properties of the composites, for instance, enhancement in conductivity and reduction in ohmic losses in the hole-selective layers and injection barriers at the interface with the electrodes, which can be achieved by controlling the energy levels of the dopants or HTMs.[126] The composite HTM, accompanied by increased charge carrier density and higher conductivity, facilitated the achievement of a high PCE.

Sang Il Seok and coworkers reported the use of *tert*-butyl-CuPC (CuPC) used as an additive in the HTM layer of *po*-spiro-OMeTAD (*po*-spiro) in a PSC based on an $(FAPbI_3)_{0.85}(MAPbBr_3)_{0.15}$ absorbing layer.[127] This optimized "bilayer" platform achieved a high FF of 0.747, $V_{OC}$ of 1.11 V and high PCE of 18.5%, whereas the single HTM-based *po*-spiro and CuPC showed a modest FF of 0.718 and 0.663, $V_{OC}$ of 1.09 V and 1.045 V, and PCE of 17.5% and 15.2%, respectively. The improvement in the $V_{OC}$ and FF values was attributed to the incorporation of CuPC in *po*-spiro, preventing the unwanted electrons from crossing the energy barrier of *po*-spiro. Transient photovoltage decay (TPD) measurements showed that the recombination lifetime of the device with CuPC-doped *po*-spiro was higher than that of the device with single *po*-spiro HTM, suggesting that the introduction of CuPC as a dopant in the *po*-spiro HTM layer could retard charge recombination, and then result in an enhancement in FF and $V_{OC}$.

Lianos' group and our group used *n*-butyl tetra-substituted CuPc (CuBuPc, **6**) as an additive in spiro-OMeTAD in a mesoscopic perovskite device and achieved an impressive improvement in the PCE values of the PSCs.[128] This was associated with the creation of deep traps in the hole transportation and better blocking of the back-travelling electrons due to the low-lying LUMO level of CuBuPc compared to that of spiro-OMeTAD. It was also demonstrated that the presence of the Pc materials could enhance the thin film quality of spiro-OMeTAD by decreasing the size and number of pinhole defects. Accordingly, with the decreased shunt paths, the FF and $V_{OC}$ of the cells increased, leading to a PSC with PCE of 15.4% for the devices based on spiro-OMeTAD with 10% CuBuPc as the HTM. The reference device showed an efficiency of 10.4%. Liao's group developed a solution-processed composite HTM consisting of PEDOT:PSS and copper phthalocyanine-3,4′,4″,4‴-tetrasulfonated acid tetrasodium salt (TS−CuPc, **61**) and investigated its performance in PSCs with an inverted p–i–n structure.[129] The results suggested an improved cell performance and stability due to the incorporation of TS-CuPc in PEDOT:PSS. The optimized composite film of TS-CuPc-doped PEDOT:PSS (50 wt%) showed better film uniformity and lower roughness compared with the pristine PEDOT:PSS and TS-CuPc thin films. The composite HTM also offered better energy alignment for efficient hole transport and extraction. In addition, the perovskite film fabricated on the composite HTM layer offered higher crystallinity with a larger grain size, together with better film coverage and enhanced carrier mobility. Finally, PSCs with a PCE of 17.29% were achieved, while the control device using pristine PEDOT:PSS exhibited an efficiency of 13.29%. In 2018, our group studied composites based on non-peripheral octamethyl-substituted CuPc nanowire (N-$CuMe_2Pc$, **68**) and P3HT and employed them as HTMs in PSCs, reaching PCEs of up to 16.61% for the optimized weight ratio of 1 : 1.[130] The composite thin films with this optimized ratio showed both the best film quality and the highest hole mobility, resulting in a good performance. Achieving a high charge carrier mobility for P3HT requires precise control of the morphology and crystallinity of its thin film. The hole mobility of P3HT can be enhanced with optimized π–π stacking of the polymer side chain. Peng and coworkers produced a highly crystalline P3HT thin film by blending it with CuPc and employing a post-deposition solvent-annealing step with chlorobenzene.[131] According to the XRD results, a significant improvement in crystallinity and conductivity of the thin film occurred when the solvent annealing treatment was applied, and a further enhancement was observed by blending P3HT with CuPc. The devices based on the developed solution-based composite HTM achieved a high efficiency of 21.6% for an active area of 1 $cm^2$. The use of the hydrophobic and thermally stable P3HT:CuPc composite HTM could also increase the stability of the PSC devices against light, moisture and heat. The encapsulated devices could retain 91.7% of their initial performance after 1000 h of exposure to damp heat and high humidity (Fig. 10).

$NiPcS_4$ (**69**), containing four sulphonate sodium salt as peripherally attached substituents, has been used as either a dopant-free HTM or a dopant in PEDOT:PSS, and applied in inverted PSCs.[132] The addition of 10 wt% of $NiPcS_4$ to PEDOT:PSS led to PSCs with a PCE of up to 18.90%, which was significantly higher than that for the PSCs based on other components, *i.e.*, 16.47% and 9.29% for PEDOT:PSS and $NiPcS_4$, respectively. The observed improvement in the performance of PSCs was attributed to factors such as enhanced photon absorption, improved film quality of perovskite, enhanced work function of HTM and its hole transporting ability, and increased cell stability. The photovoltaic properties of some selected perovskite devices using Pc compounds as additives in the HTM layer are summarized in Table 4.[52,127–130,132]

 

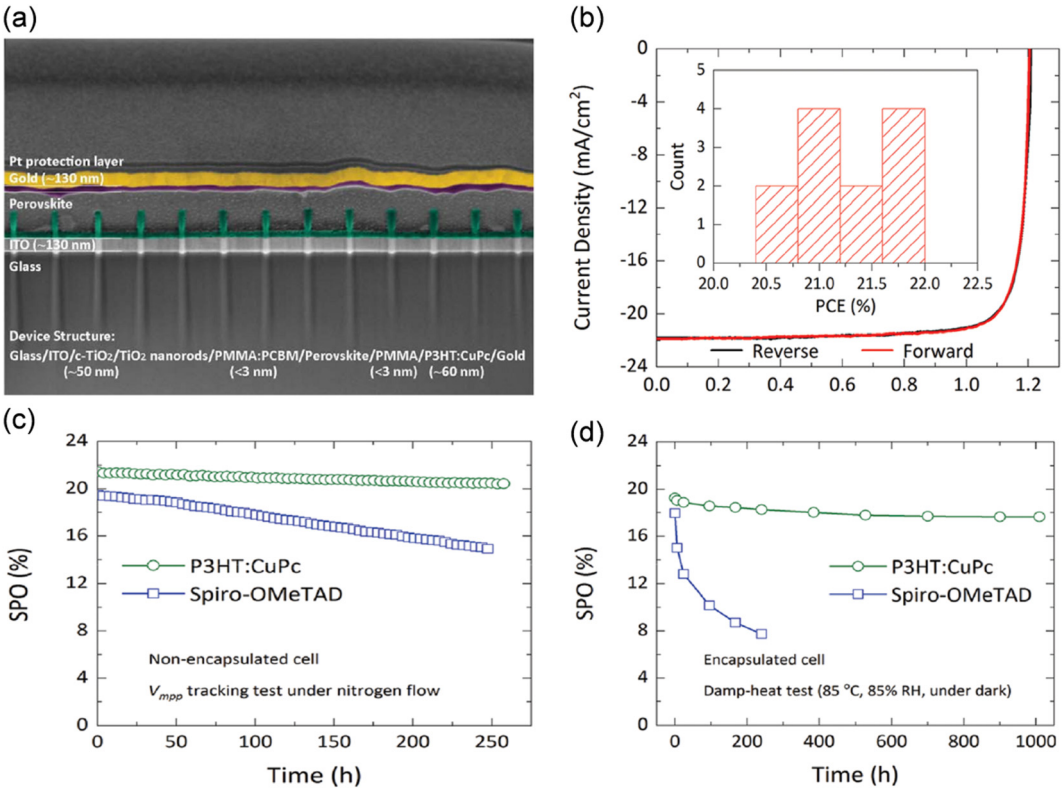


Fig. 10 (a) Cross-sectional SEM image, (b) *J*–*V* performance and (c) SPO of nonencapsulated cells based on P3HT:CuPc and spiro-OMeTAD HTL measured by Vmpp tracking under continuous 1 Sun illumination intensity. (d) SPO of encapsulated cells based on P3HT:CuPc and Spiro-OMeTAD HTL. Reproduced with permission.[131] Copyright 2021, Science.

The molecular structures of the Pc materials used as additives in HTMs or perovskite layers in PSCs are shown in Fig. 9.

### 2.5. Pc complexes using as additives in perovskite layer

In the process of fabricating polycrystalline organometal halide perovskite thin films or operation of PSCs, defects are inevitably generated in the films. These defects can be categorized as 1D point defects (vacancies, interstitial and anti-site atoms), 2D defects consisting of grain boundaries and abundant surface defects and 3D bulk crystal defects such as lead clusters.[133] These intrinsic defects, such as halide and cation vacancies, under-coordinated halide anions, lead cations, lead clusters and lead–halide antisite defects exist at the grain boundaries and surfaces, resulting in trap states, which cause non-radiative recombination of the photo-induced carriers and undesirably lower the photovoltaic parameters, and thus PCE. The hysteresis effect in the *J*–*V* curves of PSCs can also be attributed to these defects. Moreover, the instability issue of PSCs is associated with the defective grain boundaries because heat and moisture degrade the film from initiating at the surface of the film. Then, the grain boundaries filled with defects finally diffuse into the bulk perovskite.[134] The charged defects also migrate through the grain boundaries under an electrical bias.

As one of the main approaches to passivate defects in perovskite, diverse additives ranging from organic molecules to salts and polymers have achieved an inspiring improvement in the modification of PSCs. The method for the incorporation of additives in perovskite films can be classified as two types, *i.e.*, the widely adopted introduction of additives in the perovskite precursor solution and dissolving the additive in an anti-solvent such as chlorobenzene, *via* a one-step dripping process. In the former, the morphology of the perovskite film is affected by the additives given that the dopant is scattered in the precursor solution and the colloidal clusters serve as nucleation centers for the growth and crystallization of the perovskite film.[135] In the latter, the additives, in most cases, can remain in the surface of the film, influencing the surface or grain boundaries of perovskite films.[136] Therefore, the additive engineering strategy can be utilized for the modulation of the morphology of perovskite films, the dimensionality of the perovskite, the band alignment, the durability of the harvesting layer and passivation of the defects, or realization of the combination of all of them.[137,138] Many compounds as additives employed in PSC have been reported. However, the introduction of Pc as an additive in perovskite is rare to date and its application is in its infancy.

Unsubstituted CuPc has been used as an additive in perovskite or an interlayer to modify the surface and tailor the interfacial structure in PSCs. Behjat *et al.* added different amounts of CuPc to the perovskite material in PSCs and achieved higher $J_{SC}$ values for the devices using 0.05 wt% of CuPc in $CH_3NH_3PbI_3$.[139] It has been suggested that CuPc can

Table 4 Photovoltaic properties of some selected perovskite devices employing Pc compounds as additives in the HTM layer or perovskite layer

| Chemical structures no. | Device architecture | HTM | Additive | Hole mobility of HTM ($cm^2\ V^{-1}\ s^{-1}$) | $V_{OC}$ (V) | $J_{SC}$ ($mA\ cm^{-2}$) | FF (%) | PCE (%) | Ref. |
|---|---|---|---|---|---|---|---|---|---|
| **66** | Planar n–i–p | spiro-OMeTAD | Zn S2 | | 1.012 | 22.57 | 71.45 | 16.64 | 52 |
| **67** | Planar n–i–p | spiro-OMeTAD | Zn S3 | | 1.033 | 22.75 | 76.55 | 18.01 | 52 |
| **6** | Mesoscopic | spiro-OMeTAD | *n*-BuPc | | 0.97 | 24.9 | 64 | 15.4 | 128 |
| **71** | Planar p–i–n | PEDOT:PSS | TS-CuPc | | 1.01 | 22.23 | 77 | 17.29 | 129 |
| **68** | Planar n–i–p | P3HT | N-$CuMe_2$Pc | $3.84 \times 10^{-3}$ | 1.008 | 22.44 | 73.43 | 16.61 | 130 |
| **69** | Planar p–i–n | PEDOT:PSS | $NiPcS_4$ | | 1.08 | 23.01 | 77 | 18.90 | 132 |
| **5** | Mesoscopic | po-spiro-OMeTAD | *t*-BuPc | | 1.11 | 22.3 | 74.7 | 18.5 | 127 |
| | Mesoscopic | spiro-OMeTAD | CuPc | | 0.88 | 15.30 | 61.7 | 8.4 | 139 |
| **5** | Planar n–i–p | spiro-OMeTAD | *t*-BuCuPc | | 1.02 | 22.6 | 75 | 17.3 | 141 |
| | Planar n–i–p | spiro-OMeTAD | NiPc | | 1.10 | 23.29 | 74.78 | 19.18 | 140 |
| **70** | Planar p–i–n | PTAA | HCuPc | | 1.032 | 25.57 | 81.05 | 21.39 | 142 |
| **71** | Mesoscopic | cobalt porphyrin | tetra-$NH_2$-ZnPc | | 1.11 | 23.55 | 77.28 | 20.3 | 144 |
| | Mesoscopic | spiro-OMeTAD | CuPc | | 1.112 | 22.7 | 78 | 19.7 | 143 |
| **72** | Mesoscopic | spiro-OMeTAD | $F_{16}$CuPc | | 1.145 | 22.9 | 77 | 20.2 | 143 |
| **73** | Mesoscopic | spiro-OMeTAD | FeTAP | | 1.11 | 23.78 | 73.26 | 18.81 | 146 |
| **74** | Planar n–i–p | spiro-OMeTAD | 8TPAEPC | | 1.123 | 24.0 | 82.00 | 22.10 | 147 |
| **75** | Planar n–i–p | spiro-OMeTAD | NP-$SC_6$-ZnPc | | 1.09 | 23.18 | 71.4 | 18.04 | 145 |
| **41** | Planar n–i–p | spiro-OMeTAD | NP-$SC_6$-TiOPc | | 1.12 | 23.27 | 74.4 | 19.39 | 145 |

improve the quality of the perovskite thin film and enhance its light absorption ability. The addition of CuPc to the perovskite increased the PCE of the device by 2% compared to the reference device with no CuPc in the perovskite layer. Also, spiro-OMeTAD was used as the HTM in this study, and the highest efficiency of 8.4% was achieved for the PSCs. Jin *et al.* improved the PCE of their spiro-OMeTAD-based PSCs from 17.4% to 19.18% by introducing NiPc as an additive in the perovskite layer.[140] To achieve this goal, NiPc was added to the anti-solvent chlorobenzene, and subsequently infiltrated in the perovskite surface, which improved the crystal quality of the perovskite film and slightly reduce the defects on its surface, enhancing its interface with the HTM layer. The developed method effectively reduced the recombination rate and enhanced the charge extraction and transfer efficiency, leading to a higher performance for the PSCs. Peng *et al.* used a very low concentration ($4.4 \times 10^{-3}$ mM) of *t*-BuCuPc as an additive in perovskite materials in a planar PSC with a $TiO_2$ thin layer as the ETM and spiro-OMeTAD as the HTM, improving the performance of the solar cell from 15.3% to 17.3%.[141] It was found that *t*-BuCuPc could enhance the quality of the perovskite layer with higher crystallinity and surface coverage. Dong *et al.* synthesized a hyperbranched CuPc (HCuPc) (**70**) as an additive to $FAPbI_3$ perovskite.[142] The developed Pc molecules could encapsulate the grain boundaries at the molecular level through their twisted Pc units and improve the phase stability of the $FAPbI_3$ perovskite against humidity, as well as the charge extraction and transport. The p–i–n devices using HCuPc additive could achieve the remarkable efficiency of 21.39%. The photovoltaic properties of some selected perovskite devices using Pc compounds as additives in the perovskite layer are summarized in Table 4.[139–147]

Tang and coworkers explored the impact of post-treating the $MAPbI_3$ perovskite layer using tetra-ammonium-substituted ZnPc on the device performance.[144] The two-dimensional $(ZnPc)_{0.5}MA_{n-1}Pb_nI_{3n+1}$ was constructed in the grain boundaries of the $MAPbI_3$ film by immersing the as-fabricated perovskite layer in an isopropanol solution of the ZnPc derivative (**71**), resulting in the successful passivation of defects and reduced trap-assisted recombination. The modified PSCs with doped spiro-OMeTAD HTM showed improved PCEs of up to 20.3% compared with 19.01% for the reference devices, and long-term stability against humidity and heating, with self-repairing capability under mild heating. The use of the spin-coating method for the deposition of the two-dimensional $(ZnPc)_{0.5}MA_{n-1}Pb_nI_{3n+1}$ layer led to an efficiency of 19.6% for the modified PSC.[148]

Unsubstituted CuPc and its fluorinated derivative $F_{16}$CuPc (**72**) were utilized as additives in the perovskite films reported by Ma and coworkers in 2018.[143] The introduction of a dipole layer not only aligned the interfacial energy levels but also filled the grain boundaries and passivated the perovskite surface, which led to significantly suppressed charge recombination. The Pc-treated PSCs showed an improved PCE, where the best PCE was 20.2%, $V_{OC}$ was 1.145 V, $J_{SC}$ was 22.9 mA $cm^{-2}$, and FF was 0.77 for $F_{16}$CuPc, and a PCE of 19.7% coupled with $V_{OC}$ of 1.112 V, $J_{SC}$ of 22.7 mA $cm^{-2}$ and FF of 0.78 for CuPc. In comparison with the pristine device, the improvement in the PCE of the modified devices is mainly attributed to the increase in the $V_{OC}$, stemming from the reduced interfacial recombination by the introduction of CuPc and $F_{16}$CuPc in the perovskite. Furthermore, treatment with $F_{16}$CuPc and CuPc could also preserve the perovskite layer from moisture penetration to some extent. Hence, the PCE of the modified devices sacrificed 5% ($F_{16}$CuPc) and ~10% (CuPc) after 1000 h storage under atmosphere conditions without any sealing, while the control devices retained around 80% of their initial PCE. In a recent study, CuPc and $F_{16}$CuPc were studied as hole and electron transport layers in an $MAPI_3$-based PSC device, respectively, through DFT calculations and compared to the state-of-art charge transport materials $TiO_2$ and spiro-OMeTAD, suggesting that better efficiency can be achieved for the Pc-based device.[149] The device simulation study showed that an FF of 79.01% and PCE of 22.30% can be expected for this PSC device. In 2022, iron(II)-2,9,16,23-tetraamino-phthalocyanine (FeTAP) (**73**) was

 

used as an additive inside a mixed-halide perovskite layer to passivate the defects at the surface and grain boundaries through the formation of strong bonds between the unsaturated $Pb^{2+}$ ions and N–H moieties.[146] This allowed the adjacent crystal grains to be crosslinked in the perovskite film, resulting in a high-quality thin film with improved charge extraction in the device. This could additionally enhance the device stability by inhibiting the perovskite film degradation process. The best-performing FeTAP-modified device achieved the PCE of 18.81%. 8TPAEPC (**74**), a CuPc compound with eight triphenylamine groups grafted into the peripheral side of Pc, was used as the dopant for a mixed-ion perovskite film and enhanced the PCE of the perovskite devices from 20% to 22.10%.[147] As a narrow band gap additive, 8TPAEPC could extend the NIR photo-response of the perovskite film from 760 to 850 nm, which consequently enhanced the $J_{SC}$ value of the device from 22.8 to 24 mA $cm^{-2}$. It was indicated that there are electrostatic interactions between 8TPAEPC and perovskite molecules, which assisted the crystal growth of the perovskite, leading to more packed crystal grains and smoother surface in the final film. Interestingly, using the p-type 8TPAEPC as a dopant-free HTM, PSCs with a PCE of 20.42% were achieved.

In a study conducted by our research group, two types of Pc derivatives, NP-$SC_6$-ZnPc (**75**) and NP-$SC_6$-TiOPc (**41**), could successfully passivate the defects in the perovskite layer (Fig. 11).[150] The lone electron pairs on the S, N and O atoms in the Pc molecular structures provide the chance to form a coordination bond with under-coordinated $Pb^{2+}$ in $CH_3NH_3PbI_3$ together with passivating Pb–I antisite defects, which was verified by theoretical calculation and X-ray photoelectron spectroscopy (XPS) analysis. Using DFT calculations, the absorption behaviors of the Pc molecules (NP-$SC_6$-ZnPc and NP-$SC_6$-TiOPc) were investigated on the $MAPbI_3$ (001) surface. The computational results confirmed that both Pc molecules prefer to absorb on the Pb–$I_2$-terminated (001) surface, with absorption energies of −3.36 and −3.61 eV for NP-$SC_6$-ZnPc and NP-$SC_6$-TiOPc, respectively, which indicates the efficient absorption of the developed Pc molecules on the surface of $MAPbI_3$. Moreover, an increase in the absorption energies was observed when the NP-$SC_6$-ZnPc and NP-$SC_6$-TiOPc molecules point to the I atoms in $MAPbI_3$. It was also demonstrated that the formation of the strong O-Pb bond with a bond length of 2.34 Å between NP-$SC_6$-TiOPc and $MAPbI_3$ molecules may play a crucial role in the absorption of this molecule on the perovskite surface. The relaxed structures of $MAPbI_3$/NP-$SC_6$-ZnPc and $MAPbI_3$/NP-$SC_6$-TiOPc are displayed in Fig. 11. The SEM study showed that Pc passivation affected the perovskite growth and assisted the formation of more condensed, continuous and uniform perovskite films with larger grain sizes. The PSCs fabricated with Pc-decorated $CH_3NH_3PbI_3$ as the light harvesting layer showed a champion PCE of up to 19.39% and 18.04% for the NP-$SC_6$-TiOPc- and NP-$SC_6$-ZnPc-based devices, respectively, in comparison with the additive-free modified devices (17.67%). The presence of an oxygen atom coordinated to the axial position of the metal center in NP-$SC_6$-TiOPc enabled the easier formation of coordination bonds with the under-coordinated $Pb^{2+}$ and better passivation effect compared with the NP-$SC_6$-ZnPc counterpart. Furthermore, the resultant high-quality perovskite film with reduced traps and hydrophobic Pc displayed good durability both in the moisture and thermal test. Employing a thin passivation layer of the hydrophobic Pc materials on the top of the perovskite film can offer effective protection against humidity. Exposing the bare perovskite film to a high moisture level led to a color change from black to yellow after 60 s. Simultaneously, the $MAPbI_3$/NP-$SC_6$-TiOPc film showed significantly higher resistance to high humidity. Furthermore, both passivated devices showed high stability against elevated temperature. Although the control PSC lost 67% of its initial performance after increasing the temperature to 200 °C, the champion PSC with the perovskite film passivated by NP-$SC_6$-TiOPc could maintain over 80% of its initial efficiency.

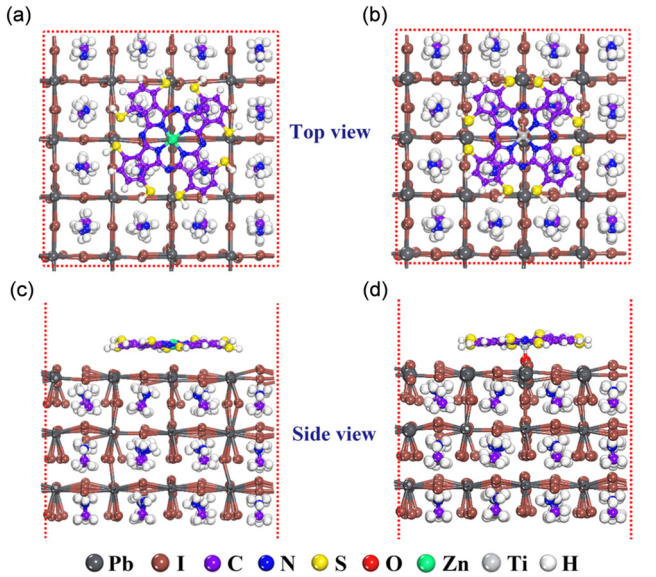


Fig. 11 (a) Top and (b) side views of $MAPbI_3$/NP-$SC_6$-ZnPc. (c) Top and (d) side views of $MAPbI_3$/NP-$SC_6$-TiOPc for relaxed structures by DFT calculation. Reproduced with permission.[150] Copyright 2021, Wiley.

## 3. Conclusion and prospects

Perovskite solar cells have experienced astounding progress in their efficiency in the last 10 years, almost approaching the Shockley–Queisser theoretical efficiency. However, their instability and the adaption of industrial-scale fabrication techniques are the two main factors hindering their commercialization. Several factors, such as thermal treatment, light illumination, and humidity, affect the stability of the devices, among which moisture is verified to be one of the leading causes of the degradation of perovskites. Li-salt-doped spiro-OMeTAD as the HTM in PSCs has achieved great success. However, the hydrophilic property of the additive induces moisture to invade the perovskite films, leading to their decomposition. Thus, to address the instability problem, numerous novel semiconducting materials have been explored to improve the stability of PSCs, while keeping the PCEs of the devices

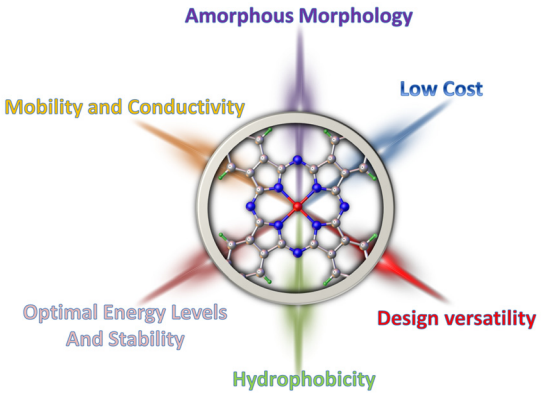


Fig. 12 Required characteristics of Pcs for minimizing the defects in perovskites or on their surface, enhancing their interfacial contact with the active layer and inhibiting the incursion of moisture.



high. Among them, phthalocyanine compounds are the most promising candidates, owing to their excellent carrier mobility, chemical/physical stability, low cost, suitable energy levels, *etc.* However, to match the industrial-scale film-coating techniques, the fabrication of thin and dense organic layers, especially small molecule-based layers, is rarely reported, which can be an upcoming research direction.

In this review, the applications of Pc materials were summarized in categories including Pcs employed in perovskite layer, functioning as passivate agents or pinhole/crack filler, and HTM layers, interfacial films and dopants in HTMs. The ultimate challenge for Pc-based PSCs is to achieve a high PCE comparable to the widely used spiro-OMeTAD, as well as a long operation time in the ambient environment. Thus, to achieve this goal, novel Pcs with the following properties (Fig. 12) should be considered to minimize the defects in perovskites or on their surface, enhance their interfacial contact with the active layer and inhibit the incursion of moisture.

(1) Low cost: newly developed materials should be cheaper with regard to both material price and production cost than the commonly used spiro-OMeTAD for their potential mass industrialization.

(2) Introducing heteroatoms or groups in the periphery of the Pc ring, as well as the axial ligands, which can act as Lewis acids/bases and passivate the perovskite defects; peripheral groups containing heteroatoms of N, O and S as well as some Lewis-base groups such as carbonyl can favor efficient hole transport and interface passivation; besides, axial ligands connected with the central metal in the Pc core can also provide the site for perovskite passivation.

(3) Good hydrophobicity: as an HTM in the device with n–i–p structure, Pc should possess both high mobility and good hydrophobicity given that it functions as not only a hole extraction and transport layer but also a capping layer to protect the perovskite film from moisture ingress. Alternatively, as an additive in perovskite for the passivation of the perovskite film or filling the cracks, moderate hydrophobicity is desirable because high hydrophobicity may cause the wetting issue in upper HTMs.

(4) Amorphous morphology: Pc films with high crystallization generally offer higher mobility but at the expense of the thin film quality. Consequently, the low film quality can have a negative effect on the charge transfer and device performance. Therefore, an amorphous film with smooth and pinhole-free morphology is a prerequisite for realizing a high performance in PSCs. Besides, a dense film also inhibits moisture flow from the ambient conditions. Regarding the solution-based deposition techniques for the fabrication of Pc films, the size and nature, and attached position of the substituents around the Pc ring can notably manipulate the solid-state interactions between Pc molecules, and therefore, should be selected wisely to balance the π–π interaction level and the spatial hinderance to form a thin film with sufficient crystallinity and good film quality with smooth surface morphology.

(5) High mobility and conductivity: the modification of peripheral substituents can alter optoelectronic and electrochemical properties of Pc, while this modulation may weaken the degree of aggregation of the Pc, which is not beneficial to achieve a high PCE in PSCs given that high conductivity and hole mobility are required in the device. In this regard, some structural engineering in Pcs should be conducted under the guidance of computational simulations, realizing π–π stacking interactions as well as high conductivities.

(6) Finally, a suitable energy level and resistance to thermal, optical, chemical, and environmental stresses.

In summary, newly designed Pcs should be closely coordinated with perovskite passivation and improved hydrophobicity for elevating the PCE and durability of PSCs. This review presented a summary of the recent progress and insights into the future development of Pc-based HTMs, and we anticipate that it can offer new insight for developing novel preeminent Pc-based semiconducting materials to further enhance the efficiency and stability of PSCs.

## Conflicts of interest

The authors declare that they have no conflict of interest.

## Acknowledgements

E. R., and D. K. contributed equally to this work. The work at the Southern University of Science and Technology was supported by the National Science Foundation of China (No. 21975116) and General Program of Basic Research in Shenzhen (JCYJ20220530112801004).

## References

1 X. Li, W. Zhang, X. Guo, C. Lu, J. Wei and J. Fang, Constructing heterojunctions by surface sulfidation for efficient inverted perovskite solar cells, *Science*, 2022, **375**, 434–437.

 

2 N.-G. Park and K. Zhu, Scalable fabrication and coating methods for perovskite solar cells and solar modules, *Nat. Rev. Mater.*, 2020, **5**, 333–350.
3 L. Duan and A. Uddin, Defects and stability of perovskite solar cells: a critical analysis, *Mater. Chem. Front.*, 2022, **6**, 400–417.
4 P. Zhao, B. J. Kim and H. S. Jung, Passivation in perovskite solar cells: a review, *Mater. Today Energy*, 2018, **7**, 267–286.
5 V. M. Le Corre, M. Stolterfoht, L. Perdigón Toro, M. Feuerstein, C. Wolff, L. Gil-Escrig, H. J. Bolink, D. Neher and L. J. A. Koster, Charge Transport Layers Limiting the Efficiency of Perovskite Solar Cells: How To Optimize Conductivity, Doping, and Thickness, *ACS Appl. Energy Mater.*, 2019, **2**, 6280–6287.
6 N. J. Jeon, J. H. Noh, W. S. Yang, Y. C. Kim, S. Ryu, J. Seo and S. I. Seok, Compositional engineering of perovskite materials for high-performance solar cells, *Nature*, 2015, **517**, 476–480.
7 Z. Zhou, S. Pang, Z. Liu, H. Xu and G. Cui, Interface engineering for high-performance perovskite hybrid solar cells, *J. Mater. Chem. A*, 2015, **3**, 19205–19217.
8 F. Wang, S. Bai, W. Tress, A. Hagfeldt and F. Gao, Defects engineering for high-performance perovskite solar cells, *npj Flexible Electron.*, 2018, **2**, 22.
9 D. Khan, X. Liu, G. Qu, A. R. Nath, P. Xie and Z.-X. Xu, Nexuses Between the Chemical Design and Performance of Small Molecule Dopant-Free Hole Transporting Materials in Perovskite Solar Cells, *Small*, 2023, 2205926.
10 A. A. Said, J. Xie and Q. Zhang, Recent Progress in Organic Electron Transport Materials in Inverted Perovskite Solar Cells, *Small*, 2019, **15**, 1900854.
11 P. Murugan, T. Hu, X. Hu and Y. Chen, Advancements in organic small molecule hole-transporting materials for perovskite solar cells: past and future, *J. Mater. Chem. A*, 2022, **10**, 5044–5081.
12 K. Akaike and K. Kanai, in *Physics and Chemistry of Carbon-Based Materials: Basics and Applications*, ed. Y. Kubozono, Springer Singapore, Singapore, 2019, DOI: **10.1007/978-981-13-3417-7_10**, pp. 293–332.
13 H. Lu and N. Kobayashi, Optically active porphyrin and phthalocyanine systems, *Chem. Rev.*, 2016, **116**, 6184–6261.
14 O. A. Melville, B. H. Lessard and T. P. Bender, Phthalocyanine-based organic thin-film transistors: a review of recent advances, *ACS Appl. Mater. Interfaces*, 2015, **7**, 13105–13118.
15 R. Guilard, K. M. Kadish, K. M. Smith and R. Guilard, *The porphyrin handbook*, Academic Press, New York, 2003.
16 A. B. P. Lever and C. C. Leznoff, *Phthalocyanines: properties and applications*, VCH, New York, 1996, pp. 1989–c1996.
17 O. Inganas, Organic Photovoltaics over Three Decades, *Adv. Mater.*, 2018, **30**, 26.
18 H. T. Chandran, T. Liu, D. Shen, Z. Guan, M. Li, J. Antonio Zapien, S.-W. Tsang, M.-F. Lo and C.-S. Lee, A Family of Small Molecular Materials Enabling Consistently Lower Recombination Losses in Organic Photovoltaic Devices, *Sol. RRL*, 2020, **4**, 202000245.
19 M. Urbani, M. E. Ragoussi, M. K. Nazeeruddin and T. Torres, Phthalocyanines for dye-sensitized solar cells, *Coord. Chem. Rev.*, 2019, **381**, 1–64.
20 I. Mfouo-Tynga and H. Abrahamse, Cell Death Pathways and Phthalocyanine as an Efficient Agent for Photodynamic Cancer Therapy, *Int. J. Mol. Sci.*, 2015, **16**, 10228–10241.
21 C. Rodriguez-Seco, L. Cabau, A. Vidal-Ferran and E. Palomares, Advances in the Synthesis of Small Molecules as Hole Transport Materials for Lead Halide Perovskite Solar Cells, *Acc. Chem. Res.*, 2018, **51**, 869–880.
22 G. de la Torre, C. G. Claessens and T. Torres, Phthalocyanines: old dyes, new materials. Putting color in nanotechnology, *Chem. Commun.*, 2007, 2000–2015, DOI: **10.1039/B614234F**.
23 G. Bottari, G. D. La Torre, D. M. Guldi and T. Torres, Covalent and noncovalent phthalocyanine-carbon nanostructure systems: synthesis, photoinduced electron transfer, and application to molecular photovoltaics, *Chem. Rev.*, 2010, **110**, 6768–6816.
24 M. Urdampilleta, S. Klyatskaya, J. Cleuziou, M. Ruben and W. Wernsdorfer, Supramolecular spin valves, *Nat. Mater.*, 2011, **10**, 502–506.
25 M. Abel, S. Clair, O. Ourdjini, M. Mossoyan and L. Porte, Single Layer of Polymeric Fe–Phthalocyanine: An Organometallic Sheet on Metal and Thin Insulating Film, *J. Am. Chem. Soc.*, 2011, **133**, 1203–1205.
26 O. Matsushita, V. M. Derkacheva, A. Muranaka, S. Shimizu, M. Uchiyama, E. A. Lukyanets and N. Kobayashi, Rectangular-Shaped Expanded Phthalocyanines with Two Central Metal Atoms, *J. Am. Chem. Soc.*, 2012, **134**, 3411–3418.
27 H. Wang, D. Qi, Z. Xie, W. Cao, K. Wang, H. Shang and J. Jiang, A sandwich-type phthalocyaninato metal sextuple-decker complex: synthesis and NLO properties, *Chem. Commun.*, 2013, **49**, 889–891.
28 G. Bottari, G. D. La Torre and T. Torres, Phthalocyanine–Nanocarbon Ensembles: From Discrete Molecular and Supramolecular Systems to Hybrid Nanomaterials, *Acc. Chem. Res.*, 2015, **48**, 900–910.
29 A. Braun and J. Tcherniac, The products of the action of acet-anhydride on phthalamide, *Ber. Dtsch. Chem. Ges.*, 1907, **40**, 2709–2714.
30 H. Y. Diesbach and W. E. Dec, Quelques sel compleses des o-dinitrilcs avec le cuivreet lapyridine, *Helv. Claim.*, 1927, **10**, 886–888.
31 G. T. Byrne, R. P. Linstead and A. R. Lowe, 213. Phthalocyanines. Part II. The preparation of phthalocyanine and some metallic derivatives from o-cyanobenzamide and phthalimide, *J. Chem. Soc.*, 1934, 1017–1022, DOI: **10.1039/JR9340001017**.
32 C. E. Dent and R. P. Linstead, 215. Phthalocyanines. Part IV. Copper phthalocyanines, *J. Chem. Soc.*, 1934, 1027–1031, DOI: **10.1039/JR9340001027**.
33 C. E. Dent, R. P. Linstead and A. R. Lowe, 217. Phthalocyanines. Part VI. The structure of the phthalocyanines, *J. Chem. Soc.*, 1934, 1033–1039, DOI: **10.1039/JR9340001033**.
34 R. P. Linstead and A. R. Lowe, 214. Phthalocyanines. Part III. Preliminary experiments on the preparation of

phthalocyanines from phthalonitrile, *J. Chem. Soc.*, 1934, 1022–1027, DOI: 10.1039/JR9340001022.
35 R. P. Linstead and A. R. Lowe, 216. Phthalocyanines. Part V. The molecular weight of magnesium phthalocyanine, *J. Chem. Soc.*, 1934, 1031–1033, DOI: 10.1039/JR9340001031.
36 J. M. Robertson, 136. An X-ray study of the structure of the phthalocyanines. Part I. The metal-free, nickel, copper, and platinum compounds, *J. Chem. Soc.*, 1935, 615–621, DOI: 10.1039/JR9350000615.
37 J. M. Robertson, 255. An X-ray study of the phthalocyanines. Part II. Quantitative structure determination of the metal-free compound, *J. Chem. Soc.*, 1936, 1195–1209, DOI: 10.1039/JR9360001195.
38 J. M. Robertson and I. Woodward, 37. An X-ray study of the phthalocyanines. Part III. Quantitative structure determination of nickel phthalocyanine, *J. Chem. Soc.*, 1937, 219–230, DOI: 10.1039/JR9370000219.
39 N. Kobayashi, Dimers, trimers and oligomers of phthalocyanines and related compounds, *Coord. Chem. Rev.*, 2002, **227**, 129–152.
40 J. De Saja and M. Rodriguez-Mendez, Sensors based on double-decker rare earth phthalocyanines, *Adv. Colloid Interface Sci.*, 2005, **116**, 1–11.
41 Ş. Abdurrahmanoğlu, A. Altındal, M. Bulut and Ö. Bekaroğlu, Synthesis and electrical properties of novel supramolecular octa-phthalocyaninato-dicobalt(II)-hexazinc(II) and dicobalt(II)-dimeric-phthalocyanine with six ferrocenylimin pendant groups, *Polyhedron*, 2006, **25**, 3639–3646.
42 T. Ceyhan, A. Altındal, M. K. Erbil and Ö. Bekaroğlu, Synthesis, characterization, conduction and gas sensing properties of novel multinuclear metallo phthalocyanines (Zn, Co) with alkylthio substituents, *Polyhedron*, 2006, **25**, 737–746.
43 Ö. Bekaroğlu, *Functional Phthalocyanine Molecular Materials*, Springer, 2010, pp. 105–136.
44 Z. Li, F. Gao, Z. Xiao, X. Wu, J. Zuo, Y. J. O. Song and L. Technology, Nonlinear optical properties and excited state dynamics of sandwich-type mixed (phthalocyaninato)(Schiff-base) triple-decker complexes: effect of rare earth atom, *Opt. Laser Technol.*, 2018, **103**, 42–47.
45 W. Zhou, Z. Wen and P. Gao, Less is More: Dopant-Free Hole Transporting Materials for High-Efficiency Perovskite Solar Cells, *Adv. Energy Mater.*, 2018, **8**, 1702512.
46 J. Jiang, *Functional phthalocyanine molecular materials*, Springer, 2010.
47 D. V. Konarev, A. V. Kuzmin, Y. Nakano, M. A. Faraonov, S. S. Khasanov, A. Otsuka, H. Yamochi, G. Saito and R. N. Lyubovskaya, Coordination Complexes of Transition Metals (M = Mo, Fe, Rh, and Ru) with Tin(II) Phthalocyanine in Neutral, Monoanionic, and Dianionic States, *Inorg. Chem.*, 2016, **55**, 1390–1402.
48 M.-S. Liao, T. Kar, S. M. Gorun and S. Scheiner, Effects of peripheral substituents and axial ligands on the electronic structure and properties of iron phthalocyanine, *Inorg. Chem.*, 2004, **43**, 7151–7161.
49 Y. Feng, Q. Hu, E. Rezaee, M. Li, Z.-X. Xu, A. Lorenzoni, F. Mercuri and M. Muccini, High-Performance and Stable Perovskite Solar Cells Based on Dopant-Free Arylamine-Substituted Copper(II) Phthalocyanine Hole-Transporting Materials, *Adv. Energy Mater.*, 2019, **9**, 1901019.
50 Z. Yu, L. Wang, X. Mu, C.-C. Chen, Y. Wu, J. Cao and Y. Tang, Intramolecular Electric Field Construction in Metal Phthalocyanine as Dopant-Free Hole Transporting Material for Stable Perovskite Solar Cells with >21% Efficiency, *Angew. Chem., Int. Ed.*, 2021, **60**, 6294–6299.
51 W. Chen, H. Zhang, J. Sun, R. Ghadari, Z. Zhang, F. Pan, K. Lv, X. Sun, F. Guo and C. Shi, Molecular tailor-making of zinc phthalocyanines as dopant-free hole-transporting materials for efficient and stable perovskite solar cells, *J. Power Sources*, 2021, **505**, 230095.
52 G. Qu, D. Khan, F. Yan, A. Atsay, H. Xiao, Q. Chen, H. Xu, I. Nar and Z.-X. Xu, Reformation of thiophene-functionalized phthalocyanine isomers for defect passivation to achieve stable and efficient perovskite solar cells, *J. Energy Chem.*, 2022, **67**, 263–275.
53 G. Qu, L. Dong, Y. Qiao, D. Khan, Q. Chen, P. Xie, X. Yu, X. Liu, Y. Wang, J. Chen, X. Chen and Z.-X. Xu, Dopant-Free Phthalocyanine Hole Conductor with Thermal-Induced Holistic Passivation for Stable Perovskite Solar Cells with 23% Efficiency, *Adv. Funct. Mater.*, 2022, **32**, 2206585.
54 C. V. Kumar, G. Sfyri, D. Raptis, E. Stathatos and P. Lianos, Perovskite solar cell with low cost Cu-phthalocyanine as hole transporting material, *RSC Adv.*, 2014, **5**, 3786–3791.
55 W. Ke, D. Zhao, C. R. Grice, A. J. Cimaroli, G. Fang and Y. Yan, Efficient fully-vacuum-processed perovskite solar cells using copper phthalocyanine as hole selective layers, *J. Mater. Chem. A*, 2015, **3**, 23888–23894.
56 F. G. Zhang, X. C. Yang, M. Cheng, W. H. Wang and L. C. Sun, Boosting the efficiency and the stability of low cost perovskite solar cells by using CuPc nanorods as hole transport material and carbon as counter electrode, *Nano Energy*, 2016, **20**, 108–116.
57 N. Torabi, A. Rahnamanic, H. Amrollahi, F. Mirjalili, M. A. Sadeghzade and A. Behjat, Performance enhancement of perovskite solar cell by controlling deposition temperature of copper phthalocyanine as a dopant-free hole transporting layer, *Org. Electron.*, 2017, **48**, 211–216.
58 J. H. Han, Y. X. Tu, Z. Y. Liu, X. Y. Liu, H. B. Ye, Z. R. Tang, T. L. Shi and G. L. Liao, Efficient and stable inverted planar perovskite solar cells using dopant-free CuPc as hole transport layer, *Electrochim. Acta*, 2018, **273**, 273–281.
59 X. Y. Liu, Z. Y. Liu, B. Sun, X. H. Tan, H. B. Ye, Y. X. Tu, T. L. Shi, Z. R. Tang and G. L. Liao, All low-temperature processed carbon-based planar heterojunction perovskite solar cells employing Mg-doped rutile $TiO_2$ as electron transport layer, *Electrochim. Acta*, 2018, **283**, 1115–1124.
60 Z. Y. Liu, B. Sun, X. Y. Liu, J. H. Han, H. B. Ye, Y. X. Tu, C. Chen, T. L. Shi, Z. R. Tang and G. L. Liao, 15% efficient carbon based planar-heterojunction perovskite solar cells using a $TiO_2/SnO_2$ bilayer as the electron transport layer, *J. Mater. Chem. A*, 2018, **6**, 7409–7419.

 

61 X. Y. Liu, Z. Y. Liu, B. Sun, X. H. Tan, H. B. Ye, Y. X. Tu, T. L. Shi, Z. R. Tang and G. L. Liao, 17.46% efficient and highly stable carbon-based planar perovskite solar cells employing Ni-doped rutile $TiO_2$ as electron transport layer, *Nano Energy*, 2018, **50**, 201–211.

62 X. Y. Liu, Z. Y. Liu, H. B. Ye, Y. X. Tu, B. Sun, X. H. Tan, T. L. Shi, Z. R. Tang and G. L. Liao, Novel efficient C-60-based inverted perovskite solar cells with negligible hysteresis, *Electrochim. Acta*, 2018, **288**, 115–125.

63 T. Lei, H. Dong, J. Xi, Y. Niu, J. Xu, F. Yuan, B. Jiao, W. W. Zhang, X. Hou and Z. X. Wu, Highly-efficient and low-temperature perovskite solar cells by employing a Bi-hole transport layer consisting of vanadium oxide and copper phthalocyanine, *Chem. Commun.*, 2018, **54**, 6177–6180.

64 H. B. Ye, Z. Y. Liu, X. Y. Liu, B. Sun, X. H. Tan, Y. X. Tu, T. L. Shi, Z. R. Tang and G. L. Liao, 17.78% efficient low-temperature carbon-based planar perovskite solar cells using Zn-doped $SnO_2$ electron transport layer, *Appl. Surf. Sci.*, 2019, **478**, 417–425.

65 M. M. Tavakoli, P. Yadav, D. Prochowicz and R. Tavakoli, Efficient, Hysteresis-Free, and Flexible Inverted Perovskite Solar Cells Using All-Vacuum Processing, *Sol. RRL*, 2021, **5**, 2000552.

66 H. Kim, K. S. Lee, M. J. Paik, D. Y. Lee, S.-U. Lee, E. Choi, J. S. Yun and S. I. Seok, Polymethyl Methacrylate as an Interlayer Between the Halide Perovskite and Copper Phthalocyanine Layers for Stable and Efficient Perovskite Solar Cells, *Adv. Funct. Mater.*, 2022, **32**, 2110473.

67 A. Agresti, S. Pescetelli, S. Casaluci, A. D. Carlo, R. Lettieri and M. V. Ieee, High Efficient Perovskite Solar Cells by Employing Zinc-Phthalocyanine as Hole Transporting Layer, *IEEE Int. Conf. Nanotechnol.*, 2015, 732–735.

68 A. Ioakeimidis, C. Christodoulou, M. Lux-Steiner and K. Fostiropoulos, Effect of $PbI_2$ deposition rate on two-step PVD/CVD all-vacuum prepared perovskite, *J. Solid State Chem.*, 2016, **244**, 20–24.

69 C. Chen, H. Li, J. Jin, Y. Cheng, D. Liu, H. Song and Q. Dai, Highly enhanced long time stability of perovskite solar cells by involving a hydrophobic hole modification layer, *Nano Energy*, 2017, **32**, 165–173.

70 M. Haider, C. Zhen, T. T. Wu, G. Liu and H. M. Cheng, Boosting efficiency and stability of perovskite solar cells with nickel phthalocyanine as a low-cost hole transporting layer material, *J. Mater. Sci. Technol.*, 2018, **34**, 1474–1480.

71 M. Haider, C. Zhen, T. T. Wu, J. B. Wu, C. X. Jia, G. Liu and H. M. Cheng, Nickel phthalocyanine as an excellent hole-transport material in inverted planar perovskite solar cells, *Chem. Commun.*, 2019, **55**, 5343–5346.

72 F. Hou, F. Jin, B. Chu, Z. Su, Y. Gao, H. Zhao, P. Cheng, J. Tang and W. Li, Hydrophobic hole-transporting layer induced porous $PbI_2$ film for stable and efficient perovskite solar cells in 50% humidity, *Solar Energy Mater. Solar Cells*, 2016, **157**, 989–995.

73 G. Sfyri, C. V. Kumar, Y. L. Wang, Z. X. Xu, C. A. Krontiras and P. Lianos, Tetra methyl substituted Cu(II) phthalocyanine as alternative hole transporting material for organometal halide perovskite solar cells, *Appl. Surf. Sci.*, 2016, **360**, 767–771.

74 Y. Wang, X. Liu, H. Shan, Q. Chen, T. Liu, X. Sun, D. Ma, Z. Zhang, J. Xu and Z.-X. Xu, Tetra-alkyl-substituted copper(II) phthalocyanines as dopant-free hole-transport layers for planar perovskite solar cells with enhanced open circuit voltage and stability, *Dyes Pigm.*, 2017, **139**, 619–626.

75 X. Liu, Y. Wang, E. Rezaee, Q. Chen, Y. Feng, X. Sun, L. Dong, Q. Hu, C. Li and Z.-X. Xu, Tetra-Propyl-Substituted Copper(II) Phthalocyanine as Dopant-Free Hole Transporting Material for Planar Perovskite Solar Cells, *Sol. RRL*, 2018, **2**, 1800050.

76 C. Li, Q. Hu, Q. Chen, W. Yu, J. Xu and Z.-X. Xu, Tetrapropyl-substituted palladium phthalocyanine used as an efficient hole transport material in perovskite solar cells, *Org. Electron.*, 2021, **88**, 106018.

77 G. Sfyri, Q. Chen, Y. W. Lin, Y. L. Wang, E. Nouri, Z. X. Xu and P. Lianos, Soluble butyl substituted copper phthalocyanine as alternative hole-transporting material for solution processed perovskite solar cells, *Electrochim. Acta*, 2016, **212**, 929–933.

78 E. Nouri, Y.-L. Wang, Q. Chen, J.-J. Xu, G. Paterakis, V. Dracopoulos, Z.-X. Xu, D. Tasis, M. R. Mohammadi and P. Lianos, Introduction of Graphene Oxide as Buffer Layer in Perovskite Solar Cells and the Promotion of Soluble *n*-Butyl-substituted Copper Phthalocyanine as Efficient Hole Transporting Material, *Electrochim. Acta*, 2017, **233**, 36–43.

79 E. Nouri, M. R. Mohammadi, Z. X. Xu, V. Dracopoulos and P. Lianos, Improvement of the photovoltaic parameters of perovskite solar cells using a reduced-graphene-oxide-modified titania layer and soluble copper phthalocyanine as a hole transporter, *Phys. Chem. Chem. Phys.*, 2018, **20**, 2388–2395.

80 Y. C. Kim, T. Y. Yang, N. J. Jeon, J. Im, S. Jang, T. J. Shin, H. W. Shin, S. Kim, E. Lee, S. Kim, J. H. Noh, S. I. Seok and J. Seo, Engineering interface structures between lead halide perovskite and copper phthalocyanine for efficient and stable perovskite solar cells, *Energy Environ. Sci.*, 2017, **10**, 2109–2116.

81 T. Duong, J. Peng, D. Walter, J. Xiang, H. P. Shen, D. Chugh, M. Lockrey, D. Y. Zhong, J. T. Li, K. Weber, T. P. White and K. R. Catchpole, Perovskite Solar Cells Employing Copper Phthalocyanine Hole-Transport Material with an Efficiency over 20% and Excellent Thermal Stability, *ACS Energy Lett.*, 2018, **3**, 2441–2448.

82 Y. M. Feng, Q. Chen, L. Dong, Z. H. Zhang, C. Li, S. H. Yang, S. Y. Cai and Z. X. Xu, Carbon-chain length substituent effects on Cu(II) phthalocyanines as dopant-free hole-transport materials for perovskite solar cells, *Sol. Energy*, 2019, **184**, 649–656.

83 X. Jiang, Z. Yu, H.-B. Li, Y. Zhao, J. Qu, J. Lai, W. Ma, D. Wang, X. Yang and L. Sun, A solution-processable copper(II) phthalocyanine derivative as a dopant-free

hole-transporting material for efficient and stable carbon counter electrode-based perovskite solar cells, *J. Mater. Chem. A*, 2017, **5**, 17862–17866.

84 X. Q. Jiang, D. P. Wang, Z. Yu, W. Y. Ma, H. B. Li, X. C. Yang, F. Liu, A. Hagfeldt and L. C. Sun, Molecular Engineering of Copper Phthalocyanines: A Strategy in Developing Dopant-Free Hole-Transporting Materials for Efficient and Ambient-Stable Perovskite Solar Cells, *Adv. Energy Mater.*, 2019, **9**, 9.

85 Y. Feng, Q. Hu, E. Rezaee, M. Li, Z. Xu, A. Lorenzoni, F. Mercuri and M. Muccini, High-Performance and Stable Perovskite Solar Cells Based on Dopant-Free Arylamine-Substituted Copper(II) Phthalocyanine Hole-Transporting Materials, *Adv. Energy Mater.*, 2019, **9**, 1901019.

86 J.-J. Guo, Z.-C. Bai, X.-F. Meng, M.-M. Sun, J.-H. Song, Z.-S. Shen, N. Ma, Z.-L. Chen and F. Zhang, Novel dopant-free metallophthalocyanines based hole transporting materials for perovskite solar cells: the effect of core metal on photovoltaic performance, *Solar Energy*, 2017, **155**, 121–129.

87 J.-J. Guo, X.-F. Meng, J. Niu, Y. Yin, M.-M. Han, X.-H. Ma, G.-S. Song and F. Zhang, A novel asymmetric phthalocyanine-based hole transporting material for perovskite solar cells with an open-circuit voltage above 1.0 V, *Synth. Metals*, 2016, **220**, 462–468.

88 J. J. Guo, X. F. Meng, H. W. Zhu, M. M. Sun, Y. B. Wang, W. N. Wang, M. Y. Xing and F. Zhang, Boosting the performance and stability of perovskite solar cells with phthalocyanine-based dopant-free hole transporting materials through core metal and peripheral groups engineering, *Org. Electron.*, 2019, **64**, 71–78.

89 S. Wu, Y. Zheng, Q. Liu, R. Li and T. Peng, Low cost and solution-processable zinc phthalocyanine as alternative hole transport material for perovskite solar cells, *RSC Adv.*, 2016, **6**, 107723–107731.

90 G. Zanotti, G. Mattioli, A. M. Paoletti, G. Pennesi, D. Caschera, N. Maman, I. Visoly-Fisher, R. K. Misra, L. Etgar and E. A. Katz, A Solution-Processed Tetra-Alkoxylated Zinc Phthalocyanine as Hole Transporting Material for Emerging Photovoltaic Technologies, *Int. J. Photoenergy*, 2018, 2473152.

91 L. Dong, Q. Hu, E. Rezaee, Q. Chen, S. Yang, S. Cai, B. Liu, J.-H. Pan and Z.-X. Xu, Dopant-Free Hole-Transporting Layer Based on Isomer-Pure Tetra-Butyl-Substituted Zinc(II) Phthalocyanine for Planar Perovskite Solar Cells, *Sol. RRL*, 2019, **3**, 1900119.

92 Z. D. Cui, Y. Q. Wang, Y. Chen, X. Z. Chen, X. L. Deng, W. C. Chen and C. W. Shi, Soluble tetra-methoxyltriphenylamine substituted zinc phthalocyanine as dopant-free hole transporting materials for perovskite solar cells, *Org. Electron.*, 2019, **69**, 248–254.

93 P. Qi, F. Zhang, X. Li, Y. Xiao, J. Guo and S. Wang, 2,9,16,23-Tetrakis(7-coumarinoxy-4-methyl)-metallophthalocyanines-based hole transporting material for mixed-perovskite solar cells, *Synth. Met.*, 2017, **226**, 1–6.

94 P. Huang, A. Hernández, S. Kazim, J. Follana-Berná, J. Ortiz, L. Lezama, Á. Sastre-Santos and S. Ahmad, Asymmetrically Substituted Phthalocyanines as Dopant-Free Hole Selective Layers for Reliability in Perovskite Solar Cells, *ACS Appl. Energy Mater.*, 2021, **4**, 10124–10135.

95 S. W. Kim, G. Kim, C. S. Moon, T. Y. Yang and J. Seo, Metal-Free Phthalocyanine as a Hole Transporting Material and a Surface Passivator for Efficient and Stable Perovskite Solar Cells, *Small Methods*, 2021, **5**, 2001248.

96 W. C. Chen, H. Y. Zhang, J. J. Sun, R. Ghadari, Z. G. Zhang, F. Pan, K. Lv, X. Sun, F. L. Guo and C. W. Shi, Molecular tailor-making of zinc phthalocyanines as dopant-free hole-transporting materials for efficient and stable perovskite solar cells, *J. Power Sources*, 2021, **505**, 230095.

97 G. Yang, Y.-L. Wang, J.-J. Xu, H.-W. Lei, C. Chen, H.-Q. Shan, X.-Y. Liu, Z.-X. Xu and G.-J. Fang, A facile molecularly engineered copper(II) phthalocyanine as hole transport material for planar perovskite solar cells with enhanced performance and stability, *Nano Energy*, 2017, **31**, 322–330.

98 X. Zheng, Y. Wang, J. Hu, G. Yang, Z. Guo, J. Xia, Z. Xu and G. Fang, Octamethyl-substituted Pd(II) phthalocyanine with long carrier lifetime as a dopant-free hole selective material for performance enhancement of perovskite solar cells, *J. Mater. Chem. A*, 2017, **5**, 24416–24424.

99 Y. L. Wang, X. L. Zheng, X. Y. Liu, Y. M. Feng, H. Q. Shan, L. Dong, G. J. Fang and Z. X. Xu, A study of different central metals in octamethyl-substituted phthalocyanines as dopant-free hole-transport layers for planar perovskite solar cells, *Org. Electron.*, 2018, **56**, 276–283.

100 Q. Hu, E. Rezaee, L. Dong, Q. Dong, H. Shan, Q. Chen, M. Li, S. Cai, L. Wang and Z.-X. Xu, Molecularly Designed Zinc(II) Phthalocyanine Derivative as Dopant-Free Hole-Transporting Material of Planar Perovskite Solar Cell with Preferential Face-on Orientation, *Sol. RRL*, 2019, **3**, 1900182.

101 F. Qi, B. Wu, J. Xu, Q. Chen, H. Shan, J. Xu and Z.-X. Xu, Non-peripherally octaalkyl-substituted nickel phthalocyanines used as non-dopant hole transport materials in perovskite solar cells, *Chin. Phys. B*, 2021, **30**, 108801.

102 X. Ding, C. Chen, L. Tao, C. Wu, M. Zheng, H. Lu, H. Xu, H. Li and M. Cheng, Dopant-free methoxy substituted copper(II) phthalocyanine for highly efficient and stable perovskite solar cells, *Chem. Eng. J.*, 2020, **387**, 124130.

103 Q. Hu, E. Rezaee, M. Li, Q. Chen, Y. Cao, M. Mayukh, D. V. McGrath and Z.-X. Xu, Molecular Design Strategy in Developing Titanyl Phthalocyanines as Dopant-Free Hole-Transporting Materials for Perovskite Solar Cells: Peripheral or Nonperipheral Substituents?, *ACS Appl. Mater. Interfaces*, 2019, **11**, 36535–36543.

104 F. Zhang, D. Bi, N. Pellet, C. Xiao, Z. Li, J. J. Berry, S. M. Zakeeruddin, K. Zhu and M. Grätzel, Suppressing defects through the synergistic effect of a Lewis base and a Lewis acid for highly efficient and stable perovskite solar cells, *Energy Environ. Sci.*, 2018, **11**, 3480–3490.

105 F. Zhang, W. Shi, J. Luo, N. Pellet, C. Yi, X. Li, X. Zhao, T. J. S. Dennis, X. Li and S. Wang, Isomer-pure bis-PCBM-assisted crystal engineering of perovskite solar cells

 

showing excellent efficiency and stability, *Adv. Mater.*, 2017, **29**, 1606806.

106 S. Dong, H. Tian, L. Huang, J. Zhang, D. Yan, Y. Geng and F. Wang, Non-Peripheral Tetrahexyl-Substituted Vanadyl Phthalocyanines with Intermolecular Cofacial π–π Stacking for Solution-Processed Organic Field-Effect Transistors, *Adv. Mater.*, 2011, **23**, 2850–2854.

107 X. Yin, Z. Song, Z. Li and W. Tang, Toward ideal hole transport materials: a review on recent progress in dopant-free hole transport materials for fabricating efficient and stable perovskite solar cells, *Energy Environ. Sci.*, 2020, **13**, 4057–4086.

108 F. J. Ramos, M. Ince, M. Urbani, A. Abate, M. Graetzel, S. Ahmad, T. Torres and M. K. Nazeeruddin, Non-aggregated Zn(II)octa(2,6-diphenylphenoxy) phthalocyanine as a hole transporting material for efficient perovskite solar cells, *Dalton Trans.*, 2015, **44**, 10847–10851.

109 K. T. Cho, K. Rakstys, M. Cavazzini, S. Orlandi, G. Pozzi and M. K. Nazeeruddin, Perovskite Solar Cells Employing Molecularly Engineered Zn(II) Phthalocyanines as Hole-transporting Materials, *Nano Energy*, 2016, **30**, 853–857.

110 K. T. Cho, M. Cavazzini, K. Rakstys, S. Orlandi, S. Paek, M. Franckevičius, H. Kanda, R. Gegevičius, Q. V. Emmanuel, G. Pozzi and M. K. Nazeeruddin, Perovskite Solar Cells: 18% Efficiency Using Zn(II) and Cu(II) Octakis(diarylamine)phthalocyanines as Hole-Transporting Materials, *ACS Appl. Energy Mater.*, 2019, **2**, 6195–6199.

111 N. Klipfel, J. Xia, P. Čulík, S. Orlandi, M. Cavazzini, N. Shibayama, H. Kanda, C. Igci, W. Li, Y.-B. Cheng, V. Jankauskas, K. Genevicius, A. M. Asiri, C. Momblona, K. Rakstys, G. Pozzi and M. K. Nazeeruddin, Zn(II) and Cu(II) tetrakis(diarylamine)phthalocyanines as hole-transporting materials for perovskite solar cells, *Mater. Today Energy*, 2022, **29**, 101110.

112 L. Caliò, J. Follana-Berná, S. Kazim, M. Madsen, H.-G. Rubahn, Á. Sastre-Santos and S. Ahmad, Cu(II) and Zn(II) based phthalocyanines as hole selective layers for perovskite solar cells, *Sustainable Energy Fuels*, 2017, **1**, 2071–2077.

113 E. Nouri, J. V. S. Krishna, C. V. Kumar, V. Dracopoulos, L. Giribabu, M. R. Mohammadi and P. Lianos, Soluble tetratriphenylamine Zn phthalocyanine as Hole Transporting Material for Perovskite Solar Cells, *Electrochim. Acta*, 2016, **222**, 875–880.

114 M. Cheng, Y. Li, M. Safdari, C. Chen, P. Liu, L. Kloo and L. Sun, Efficient Perovskite Solar Cells Based on a Solution Processable Nickel(II) Phthalocyanine and Vanadium Oxide Integrated Hole Transport Layer, *Adv. Energy Mater.*, 2017, **7**, 1602556.

115 P. Gao, K. T. Cho, A. Abate, G. Grancini, P. Y. Reddy, M. Srivasu, M. Adachi, A. Suzuki, K. Tsuchimoto, M. Gratzel and M. K. Nazeeruddin, An efficient perovskite solar cell with symmetrical Zn(II) phthalocyanine infiltrated buffering porous $Al_2O_3$ as the hybrid interfacial hole-transporting layer, *Phys. Chem. Chem. Phys.*, 2016, **18**, 27083–27089.

116 K. T. Cho, O. Trukhina, C. Roldán-Carmona, M. Ince, P. Gratia, G. Grancini, P. Gao, T. Marszalek, W. Pisula, P. Y. Reddy, T. Torres and M. K. Nazeeruddin, Molecularly Engineered Phthalocyanines as Hole-Transporting Materials in Perovskite Solar Cells Reaching Power Conversion Efficiency of 17.5%, *Adv. Energy Mater.*, 2017, **7**, 1601733.

117 X. Jiang, Z. Yu, J. Lai, Y. Zhang, N. Lei, D. Wang and L. Sun, Efficient perovskite solar cells employing a solution-processable copper phthalocyanine as a hole-transporting material, *Sci. China: Chem.*, 2017, **60**, 423–430.

118 P. Ru, E. Bi, Y. Zhang, Y. Wang, W. Kong, Y. Sha, W. Tang, P. Zhang, Y. Wu, W. Chen, X. Yang, H. Chen and L. Han, High Electron Affinity Enables Fast Hole Extraction for Efficient Flexible Inverted Perovskite Solar Cells, *Adv. Energy Mater.*, 2020, **10**, 1903487.

119 J. Sun, N. Chandrasekaran, C. Liu, A. D. Scully, W. Yin, C. K. Ng and J. J. Jasieniak, Enhancement of 3D/2D Perovskite Solar Cells Using an F4TCNQ Molecular Additive, *ACS Appl. Energy Mater.*, 2020, **3**, 8205–8215.

120 W. Q. Wu, Q. Wang, Y. Fang, Y. Shao, S. Tang, Y. Deng, H. Lu, Y. Liu, T. Li, Z. Yang, A. Gruverman and J. Huang, Molecular doping enabled scalable blading of efficient hole-transport-layer-free perovskite solar cells, *Nat. Commun.*, 2018, **9**, 1625.

121 D. Liu, Y. Li, J. Yuan, Q. Hong, G. Shi, D. Yuan, J. Wei, C. Huang, J. Tang and M.-K. Fung, Improved performance of inverted planar perovskite solar cells with F4-TCNQ doped PEDOT:PSS hole transport layers, *J. Mater. Chem. A*, 2017, **5**, 5701–5708.

122 J. M. Wang, Z. K. Wang, M. Li, C. C. Zhang, L. L. Jiang, K. H. Hu, Q. Q. Ye and L. S. Liao, Doped Copper Phthalocyanine via an Aqueous Solution Process for Normal and Inverted Perovskite Solar Cells, *Adv. Energy Mater.*, 2018, **8**, 8.

123 X. Jiang, Z. Yu, J. Lai, Y. Zhang, M. Hu, N. Lei, D. Wang, X. Yang and L. Sun, Interfacial Engineering of Perovskite Solar Cells by Employing a Hydrophobic Copper Phthalocyanine Derivative as Hole-Transporting Material with Improved Performance and Stability, *ChemSusChem*, 2017, **10**, 1838–1845.

124 M. Pegu, D. Molina, M. J. Álvaro-Martins, M. Castillo, L. Ferrer, P. Huang, S. Kazim, Á. Sastre-Santos and S. Ahmad, Dimers of diethynyl-conjugated zinc-phthalocyanine as hole selective layers for perovskite solar cell fabrication, *J. Mater. Chem. C*, 2022, **10**, 11975–11982.

125 Y. Deng, X. Zheng, Y. Bai, Q. Wang, J. Zhao and J. Huang, Surfactant-controlled ink drying enables high-speed deposition of perovskite films for efficient photovoltaic modules, *Nat. Energy*, 2018, **3**, 560–566.

126 K. Rakstys, C. Igci and M. K. Nazeeruddin, Efficiency vs. stability: dopant-free hole transporting materials towards stabilized perovskite solar cells, *Chem. Sci.*, 2019, **10**, 6748–6769.

127 J. Seo, N. J. Jeon, W. S. Yang, H.-W. Shin, T. K. Ahn, J. Lee, J. H. Noh and S. I. Seok, Effective Electron Blocking of CuPC-Doped Spiro-OMeTAD for Highly Efficient Inorganic-

Organic Hybrid Perovskite Solar Cells, *Adv. Energy Mater.*, 2015, **5**, 1501320.

128 E. Nouri, Y.-L. Wang, Q. Chen, J.-J. Xu, V. Dracopoulos, L. Sygellou, Z.-X. Xu, M. R. Mohammadi and P. Lianos, The beneficial effects of mixing spiro-OMeTAD with *n*-butyl-substituted copper phthalocyanine for perovskite solar cells, *Electrochim. Acta*, 2016, **222**, 1417–1423.

129 J.-M. Wang, Z.-K. Wang, M. Li, K.-H. Hu, Y.-G. Yang, Y. Hu, X.-Y. Gao and L.-S. Liao, Small Molecule Polymer Composite Hole-Transporting Layer for Highly Efficient and Stable Perovskite Solar Cells, *ACS Appl. Mater. Interfaces*, 2017, **9**, 13240–13246.

130 Q. Hu, E. Rezaee, Q. Dong, H. Shan, Q. Chen, L. Wang, B. Liu, J.-H. Pan and Z.-X. Xu, P3HT/Phthalocyanine Nanocomposites as Efficient Hole-Transporting Materials for Perovskite Solar Cells, *Sol. RRL*, 2019, **3**, 1800264.

131 J. Peng, D. Walter, Y. Ren, M. Tebyetekerwa, Y. Wu, T. Duong, Q. Lin, J. Li, T. Lu, M. A. Mahmud, O. L. C. Lem, S. Zhao, W. Liu, Y. Liu, H. Shen, L. Li, F. Kremer, H. T. Nguyen, D.-Y. Choi, K. J. Weber, K. R. Catchpole and T. P. White, Nanoscale localized contacts for high fill factors in polymer-passivated perovskite solar cells, *Science*, 2021, **371**, 390–395.

132 X. F. Zhang, X. Y. Zhou, L. Z. Zhang and B. M. Xu, Facile phthalocyanine doping into PEDOT leads to highly efficient and stable inverted metal halide perovskite solar cells, *J. Mater. Chem. A*, 2018, **6**, 12515–12522.

133 J. M. Ball and A. Petrozza, Defects in perovskite-halides and their effects in solar cells, *Nat. Energy*, 2016, **1**, 16149.

134 Q. Wang, B. Chen, Y. Liu, Y. Deng, Y. Bai, Q. Dong and J. Huang, Scaling behavior of moisture-induced grain degradation in polycrystalline hybrid perovskite thin films, *Energy Environ. Sci.*, 2017, **10**, 516–522.

135 M. Vasilopoulou, A. Fakharuddin, A. G. Coutsolelos, P. Falaras, P. Argitis, A. Yusoff and M. K. Nazeeruddin, Molecular materials as interfacial layers and additives in perovskite solar cells, *Chem. Soc. Rev.*, 2020, **49**, 4496–4526.

136 Y. Wu, X. Yang, W. Chen, Y. Yue, M. Cai, F. Xie, E. Bi, A. Islam and L. Han, Perovskite solar cells with 18.21% efficiency and area over 1 $cm^2$ fabricated by heterojunction engineering, *Nat. Energy*, 2016, **1**, 16148.

137 T. Zhao, C.-C. Chueh, Q. Chen, A. Rajagopal and A. K. Y. Jen, Defect Passivation of Organic–Inorganic Hybrid Perovskites by Diammonium Iodide toward High-Performance Photovoltaic Devices, *ACS Energy Lett.*, 2016, **1**, 757–763.

138 T. S. Sherkar, C. Momblona, L. Gil-Escrig, J. Avila, M. Sessolo, H. J. Bolink and L. J. A. Koster, Recombination in Perovskite Solar Cells: Significance of Grain Boundaries, Interface Traps, and Defect Ions, *ACS Energy Lett.*, 2017, **2**, 1214–1222.

139 M. Mozaffari, A. Behjat and N. Torabi, Application of copper phthalocyanin for surface modification of perovskite solar cells, *J. Mater. Sci.: Mater. Electron.*, 2018, **29**, 18187–18192.

140 S. Jin, Y. L. Wei, F. Y. Huang, X. M. Yang, D. Luo, Y. Fang, Y. Z. Zhao, Q. Y. Guo, Y. F. Huang and J. H. Wu, Enhancing the perovskite solar cell performance by the treatment with mixed anti-solvent, *J. Power Sources*, 2018, **404**, 64–72.

141 S. Wu, Q. Liu, Y. Zheng, R. Li and T. Peng, An efficient copper phthalocyanine additive of perovskite precursor for improving the photovoltaic performance of planar perovskite solar cells, *J. Power Sources*, 2017, **359**, 303–310.

142 R. Li, J. L. Ding, X. J. Mu, Y. F. Kang, A. R. Wang, W. H. Bi, Y. H. Zhang, J. Cao and Q. F. Dong, Hyperbranched phthalocyanine enabling black-phase formamidinium perovskite solar cells processing and operating in humidity open air, *J. Energy Chem.*, 2022, **71**, 141–149.

143 F. C. Li, J. Y. Yuan, X. F. Ling, L. Z. Huang, N. Rujisamphan, Y. Y. Li, L. F. Chi and W. L. Ma, Metallophthalocyanine-Based Molecular Dipole Layer as a Universal and Versatile Approach to Realize Efficient and Stable Perovskite Solar Cells, *ACS Appl. Mater. Interfaces*, 2018, **10**, 42397–42405.

144 J. Cao, X. D. Lv, X. X. Feng, R. Q. Meng, Y. Y. Wu and Y. Tang, Efficient Grain Boundary Suture by Low-Cost Tetra-ammonium Zinc Phthalocyanine for Stable Perovskite Solar Cells with Expanded Photoresponse, *J. Am. Chem. Soc.*, 2018, **140**, 11577–11580.

145 C. Li, R. He, Q. Liang, J. Cao, J. Yin and Y. Tang, 4-Tert-butylpyridine-assisted low-cost and soluble copper phthalocyanine as dopant-free hole transport layer for efficient Pb-and Sn-based perovskite solar cells, *Sci. China: Chem.*, 2020, **63**, 1053–1058.

146 K. W. Lai, C. Hanmandlu, C. C. Chang and C. W. Chu, An amino-phthalocyanine additive enhances the efficiency of perovskite solar cells through defect passivation in mixed-halide films, *Org. Electron.*, 2022, **108**, 106568.

147 Z. Zhang, H. Liu, S. Wang, H. Bao, F. Zhang and X. Li, Extended Near-Infrared Photovoltaic Responses of Perovskite Solar Cells by p-Type Phthalocyanine Derivative, *Adv. Funct. Mater.*, 2022, **32**, 2208539.

148 C. P. Li, X. D. Lv, J. Cao and Y. Tang, Tetra-ammonium Zinc Phthalocyanine to Construct a Graded 2D-3D Perovskite Interface for Efficient and Stable Solar Cells, *Chin. J. Chem.*, 2019, **37**, 30–34.

149 G. Pindolia, J. Pandya, S. Shinde and P. K. Jha, Fluorinated copper phthalocyanine as an electron transport material in perovskite solar cell, *Int. J. Energy Res.*, 2022, **46**, 15127–15142.

150 Q. Hu, E. Rezaee, W. Xu, R. Ramachandran, Q. Chen, H. Xu, T. El-Assaad, D. V. McGrath and Z. X. Xu, Dual Defect-Passivation Using Phthalocyanine for Enhanced Efficiency and Stability of Perovskite Solar Cells, *Small*, 2021, **17**, 2005216.

 